THE NORMAL BASILAR ARTERY: STRUCTURAL PROPERTIES AND MECHANICAL BEHAVIOR

A Thesis

by

BETHANY KAY WICKER

Submitted to the Office of Graduate Studies of
Texas A&M University
in partial fulfillment of the requirements for the degree of

MASTER OF SCIENCE

May 2007

Major Subject: Biomedical Engineering

THE NORMAL BASILAR ARTERY: STRUCTURAL PROPERTIES AND MECHANICAL BEHAVIOR

A Thesis

by

BETHANY KAY WICKER

Submitted to the Office of Graduate Studies of
Texas A&M University
in partial fulfillment of the requirements for the degree of

MASTER OF SCIENCE

Approved by:

Chair of Committee,	Jay Humphrey
Committee Members,	James Moore, Jr.
	Jerome Trzeciakowski
Head of Department,	Gerard Cote

May 2007

Major Subject: Biomedical Engineering

ABSTRACT

The Normal Basilar Artery: Structural Properties

and Mechanical Behavior. (May 2007)

Bethany Kay Wicker, B.S., Texas A&M University

Chair of Advisory Committee: Dr. Jay Humphrey

The leading cause of death in patients who survive subarachnoid hemorrhage (SAH) is stroke as a result of cerebral arterial vasospasm[1]. Such vasospasms involve a vasoactive response, but they remain enigmatic and no clinical treatment has proven effective in prevention or reduction[2].

Arteries remodel in response to diverse mechanical loads and chemical factors. Following SAH, the surrounding vasculature is exposed to a radically altered chemo-mechanical environment. It is our hypothesis that chemical stimuli associated with the formation of an extravascular blood clot dominates the maladaptive growth and remodeling response early on, thus leading to important structural changes. However, it is not clear which of the many chemical factors are key players in the production of vasospasm. Before an accurate picture of the etiology of vasospasm can be produced, it is imperative to gain a better understanding of the non-pathogenic cerebral vasculature. In particular, the rabbit basilar artery is a well established model for vasospasm. However, surprisingly little is known about the mechanical properties of the rabbit basilar artery.

Using an in vitro custom organ culture and mechanical testing device, acute and cultured basilar arteries from male White New Zealand specific pathogen free rabbits underwent cyclic pressurization tests at in vivo conditions and controlled levels of

myogenic tone. Sections of basilar arteries were imaged for collagen fiber orientation at 0, 40 and 80 mmHg at in vivo stretch conditions using nonlinear optical microscopy.

The nonlinear stress-strain curves provide baseline characteristics for acute and short-term culture basilar arteries. The active and passive testing creates a framework for interpreting the basal tone of arteries in our culture system. Nonlinear optical microscopy second harmonic generation provides unique microstructural information and allows imaging of live, intact arteries while maintaining in vivo geometries and conditions. Collagen fibers were found to be widely distributed about the axial direction in the adventitial layer and narrowly distributed about the circumferential direction in the adventitial layer. The quantified collagen fiber angles within the artery wall further support the development of accurate mathematical models.

TABLE OF CONTENTS

Page

Page

LIST OF TABLES

TABLE Page

LIST OF FIGURES

FIGURE Page

INTRODUCTION

The leading cause of death in patients who survive subarachnoid hemorrhage (SAH) is stroke as a result of cerebral arterial vasospasm[1]. Cerebral vasospasm is the delayed and prolonged constriction of cerebral blood vessels that typically occurs 3-5 days post SAH. Approximately 70% of patients presenting with SAH will experience some level of vasospasm[6]. Such vasospasms involve a vasoactive response, but they remain enigmatic and no clinical treatment has proven effective in prevention or reduction[2]. Despite the latest treatments, nearly 50% of patients will develop infarction and 15-20% will sustain a disabling stroke or die of progressive ischemia[5].

Arteries remodel in response to diverse mechanical loads and chemical factors. Following SAH, the surrounding vasculature is exposed to a radically altered chemo-mechanical environment. Figure 1 is a schematic depiction of several of the alterations to the chemical and mechanical environment seen in vasospasm. Changes in pressures and axial loads result in dilations/constrictions as well as altered rates of growth and remodeling. The cerebral spinal fluid (CSF) in vasospasm patients displays elevated levels of many smooth muscle mitogens and vasoactive molecules, in large part due to the extravascular clot formation. Amongst the key molecules associated with the clot are thrombin, endothelin-1 (ET-1), and platelet-derived growth factor (PDGF)[1,9,10]. These factors are strong vasoconstrictors as well as smooth muscle mitogens; they promote, in part, a maladaptive growth and remodeling of the vessels. In addition to the chemical factors, vasospastic vessels are known to exhibit endothelial dysfunction and vascular smooth muscle dedifferentiation and proliferation[11].

This thesis follows the style of *Journal of Vascular Research.*

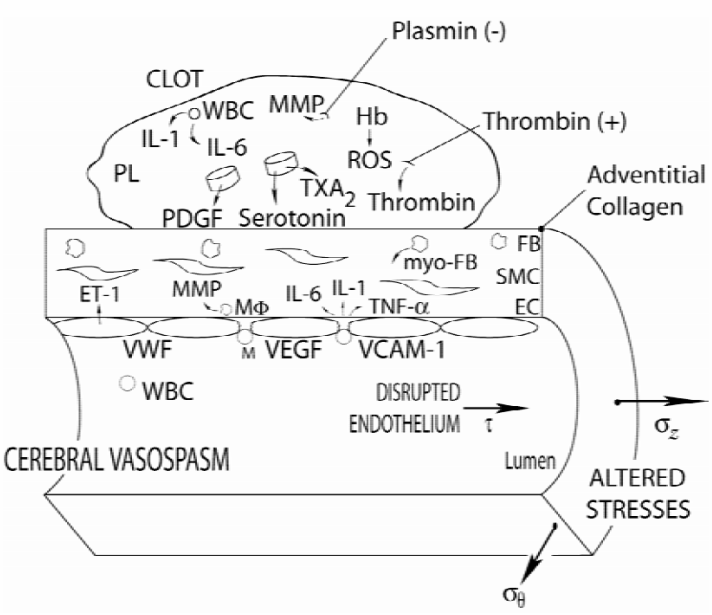

Fig. 1: Schematic of post-SAH environment showing altered chemical and mechanical environment. Note the heightened levels of growth factors and smooth muscle mitogens, as well as the disrupted endothelium and altered wall stresses.

It is our hypothesis that chemical stimuli associated with the formation of an extravascular blood clot dominates the maladaptive growth and remodeling response early on, thus leading to important structural changes and prolonged constriction in the vessels near the hemorrhage. The peak of vasospasm severity (4-7 days post SAH) and the subsequent recovery of vasospastic vessels to near normal diameters (28 days post SAH) coincide directly with the clot formation and dissolution[7]. It is this remodeling of the vessel that we believe hinders the vessel's reactivity to vasodilators (a commonly used treatment) and its response to increased shear stresses. However, it is not clear which of the many chemical factors are key players in the production of vasospasm.

There is a general consensus in the current literature implicating the involvement of alterations in the stiffness of the passive structural components, the mechanical responses of the vascular smooth muscle, and the elevated chemical factors in the

development of cerebral vasospasm. The exact etiology of the condition, however, has yet to be fully established. The need to understand such a complex and dynamic pathogenesis necessitates a more complete understanding of the non-pathogenic cerebral vasculature. Numerous studies have focused on the cerebral vasculature, yet much remains to be determined. In particular, the rabbit basilar artery is a well established model for vasospasm. However, surprisingly little is known about the mechanical properties of the rabbit basilar artery.

BACKGROUND

Proposed Vasospasm Mechanism

A proposed mechanism for cerebral arterial vasospasm is shown in Figure 2. Part A of this diagram shows a normal artery. This artery is then exposed to blood from the subarachnoid hemorrhage and the factors produced by the ensuing blood clot. Part B shows the initially vasoconstricted configuration. The blood clot then progresses and the artery remodels, possibly resulting in a thicker wall (part C). The vessel can then take two different directions. One such path is where vessel undergoes further growth, remodeling, and vasoconstriction (part D). This pathway can lead to stroke and death. The vessel could also take the path to part E where the clot dissolves and allows the flow-induced shear stresses to dilate the wall via an increased production of vasodilators. The vessel could possibly even return to the normal configuration. In order to find a way to block the path to part D we must first determine what mediates the progression from A to C.

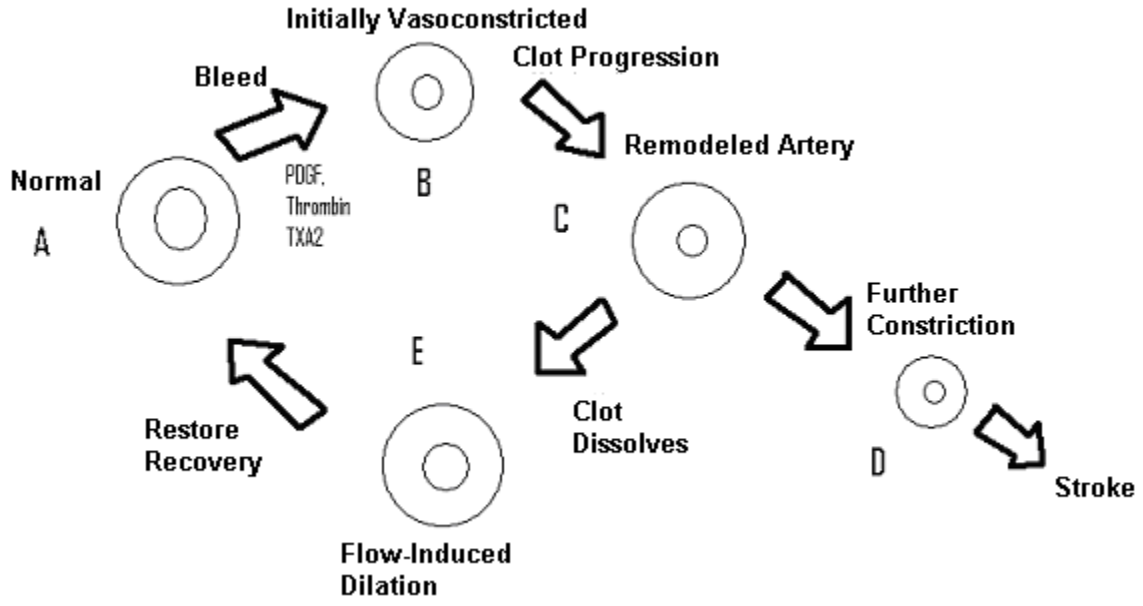

Fig. 2: Proposed mechanism for vasospasm. A shows the normal cerebral artery. B is the initially vasoconstricted artery after exposure to the blood and mitogens. C shows a partially remodeled artery after clot progression. D represents further constriction of the artery leading to stroke. E displays the opening of the artery after the clot dissolves and the shear stresses are allowed to dilate the wall.

Mechanics and Vasospasm

The alteration in mechanical behavior of vasospastic vessels has been reported in the literature over the last 30 years. In related studies, Nagasawa et al.[17,18] investigated the stiffness, β (Equation 1), incremental elastic modulus, E_{inc} (Equation 2), and the tangential mid-wall stress and strain (Equations 3 and 4, respectively) of human autopsied vasospasm patients as well as a canine SAH model. Pressure-diameter curves were recorded under passive, basal, and maximally contracted conditions induced with 50 mM KCl[18].

$$\ln\left(\frac{P_i}{P_S}\right) = \beta\left(\frac{R_0}{R_S} - 1\right) \qquad (1)$$

$$E_{inc} = \frac{\partial P_i}{\partial R_0}\frac{2\left(1-\nu^2\right)R_i{}^2 R_0}{\left(R_0{}^2 - R_i^2\right)} \qquad (2)$$

Note P_i is the intraluminal pressure, R_0 is the external radius, R_i is the internal radius and < is Poisson's ratio (taken as 0.5). The stiffness parameter shown in Equation 2 was evaluated only within the physiological pressure range of 60-180 mmHg, with P_S representing the standard pressure (100 mmHg), and R_S as the external radius at the standard pressure.

$$\varepsilon_m = \frac{\left[\left(R_0 - R_i\right)/2\right]}{\left[\left(r_0 - r_i\right)/2\right]} - 1 \qquad (3)$$

$$\sigma = \frac{P_i R_i}{\left(R_0 - R_i\right)} \qquad (4)$$

In these equations r_0 and r_i are the external radius and internal radius, respectively, at 0 mmHg under passive conditions.

The pressure-diameter curves of the human control arteries and the human SAH arteries both shifted toward the pressure axis and had sharp flexion points after KCl-induced vasoconstriction. The flexion point of the control arteries, however, was significantly lower (~20 mmHg) than that of the SAH arteries (~180 mmHg). As the intraluminal pressure increased, the E_{inc} in the active control group did not decrease until the pressure reached around 20-50 mmHg (near the flexion point). The SAH active arteries had a much higher E_{inc} than the passive arteries but it began to decline around 100-150 mmHg, which is somewhat lower than its flexion point. In the canine model the incremental elastic modulus was found to decrease dramatically on the second day after induced SAH, then recover gradually[17]. Inducing hypertension to a level above the flexion point to prompt vessel relaxation has been integrated into some severe vasospasm treatments[6].

In a double hemorrhage SAH canine model[16], basilar arteries were tested 8 days post SAH to measure the variation in smooth muscle properties and to ascertain whether enhanced passive structure rigidity contributes to vasospasm. Here, however, the basilar arteries were not tested as cylindrical segments but as 4 mm long rings with and without their endothelium. To determine the mechanics of the non-contractile component of the vessel wall, the compliance was measured during incremental loading. Compliance (Equation 5) is the inverse of the incremental elastic modulus discussed earlier and was calculated via

$$Compliance = \frac{(L - L')}{(T - T')} \qquad (5)$$

In this equation, T is the tension at length L and T' is the tension at length L'.

The compliance of the SAH group decreased significantly at 0.8 and 1.2 mm, indicating a significant stiffening after vasospasm onset. The removal of the endothelium caused a significant increase in the compliance of the control arteries, but not in the SAH arteries.

The mechanical behavior of the vessel wall is dependent not only on the wall constituents, but also on the contractile function of the smooth muscle cells. In evaluation of the mechanical behavior alterations seen in vasospasm, it is essential to determine whether the cause is changes in the arterial wall or altered vascular smooth muscle contraction. The severe (>50%) reduction in diameter in vasospastic vessels extends beyond the normal maximal contraction of the vascular wall (~30%), suggesting an increase in contractile capacity/responsiveness; alterations that could be due to important structural changes (growth and remodeling) or altered smooth muscle contractile function.

Diameter response ($\frac{\Delta D_m}{D_m}$, Equation 6) can be used as an indicator of the smooth muscle's ability to constrict an artery at given pressure levels[18]

$$\frac{\Delta D_m}{D_m} = \frac{\left[\left(D_m\right)_{ss} - \left(D_m\right)_{krs}\right]}{\left(D_m\right)_{ss}} \qquad (6)$$

D_m is the mid-wall diameter, $\left(D_m\right)_{krs}$ and $\left(D_m\right)_{ss}$ are the mid-wall diameters in the Krebs-Ringer Solution (active) and the saline solution (passive), respectively. Maximum diameter responses were generated at or near the flexion points of the pressure diameter curves.

Nagasawa et al.[15] sought to determine the contractility of the artery after SAH through testing vessels from a canine vasospasm model in saline (passive), Krebs-Ringer (active, basal), and serotonin (5-HT, 10^{-5} M, maximally contracted) solutions. Active stresses (Equations 7 and 8) in both the Krebs-Ringer, $\Delta\sigma_{krs}$, and serotonin solution, σ_{5HT}, were calculated via

$$\Delta\sigma_{krs} = \sigma_{krs} - \sigma_{ss} \qquad (7)$$

$$\Delta\sigma_{5HT} = \sigma_{5HT} - \sigma_{ss} \qquad (8)$$

with σ_{krs}, σ_{ss}, and σ_{5HT} as the wall stresses developed at given strain levels under Krebs-Ringer, saline, and 5-HT solution conditions, respectively. The canine model produced a diameter response in Krebs-Ringer and 5-HT that increased, reaching a maximum on the 7th day, thereafter recovering to the control value by the 28th day (Table 1). The 7th day also saw the development of the maximum active stress. Concerning the contractility of the vessel, spastic arteries were found to maintain their contractile response to serotonin, but as the vasospasm advanced there was an increase in the

contractile capacity of the wall. The contraction of the wall was also found to be more efficient when the arterial wall was less stiff. It was suggested that the initial decrease in stiffness of the arterial wall seen early in vasospasm could be one of the vasospasm-promoting factors. Kim et al.[16] also reported contractile function alterations post SAH. Tests on SAH arterial rings displayed considerably shorter lengths for maximal contraction and an increase in resting tension. The maximal contractions in response to KCl and UTP were also smaller in SAH arterial rings when compared to control rings, suggesting either a higher tonic level of contraction or a decreased ability of the contractile structure of the vessel wall to respond. Observed endothelial dysfunction further complicates the balance between constriction and relaxation, inhibiting the vessels ability to relax in response to vasodilators and increased shear[11].

Like the mechanical aspects, the molecular contribution to vasospasm also remains uncertain. After a subarachnoid hemorrhage, the blood introduced into the cerebral spinal fluid has several effects. The coagulation of the blood into a clot results in the activation of platelets and the subsequent release of potent growth factors.

It has been suggested that the structural changes exhibited in the cerebral blood vessels during vasospasm (smooth muscle and myofibroblast proliferation, cellular necrosis and remodeling, collagen deposition and fibrosis) are a possible cause of arterial wall thickening and decreased vessel compliance, prolonging the vasospasm period[1]. Vascular mitogens are at higher levels in the CSF after SAH in conjunction with the perivascular clot presence and confirmed cellular proliferation[1]. Borel et al.[1] confirmed significantly higher levels of PDGF-AB in the CSF of patients during the first week after SAH. Endothelin-1 and thrombin are also present in higher levels during the critical

period after SAH[9, 10]. Smooth muscle dedifferentiation to the synthetic phenotype has also been confirmed in vasospastic vessels[11], indicating the importance of approaching the vasospastic process as one of maladaptive growth and remodeling.

Motivated by the elevated immunoreactivity for PDGF-BB in endothelial cells and smooth muscle after SAH, Yanamoto et al.[14] further explored the role of PDGF in vasospasm. This study suggested that timeline associated with the production and accumulation of PDGF-BB in the smooth muscle post SAH could explain why vasospasm is delayed as well as prolonged. Thrombin is also of some interest in vasospasm as it is not only involved in the stimulation of cell proliferation, but is a known potent vasoconstrictor. Molecular marker levels for thrombin in the CSF after SAH correlate well with both the start of vasospasm and its clinical severity[14]. Knoepp et al.[13] suggested a supercedence of thrombin-induced contraction of vascular smooth muscle over transient vasorelaxants like nitric oxide (NO).

If vasospasm is to be approached and interpreted in the framework of a maladaptive growth and remodeling process, careful attention must be placed on structural alterations within the wall and their time-courses. Changes in the connective tissues and smooth muscle cells can have important functional and mechanical implications[17]. Table 1 displays structural changes in vasospastic vessels from onset to recovery[7,17].

Table 1. Summary of diameter responses shown by Kuwayama et al.[7] and Nagasawa et al. [17], connective tissue composition, wall thickness and internal radii.

	Control	2 days	4 days	7 days	14 days	28 days
Decreased Angio-Diameter[7]	0	37%	49%	20%	5%	NA
Active Diameter Response[17]	2%	5%	6%	19%	6%	1%
Collagen to Elastin Ratio	5.1	1.6	2.1	2.7	3.5	4.3
h/a @100 mmHg	0.0588	0.0588	0.0488	0.0488	0.0525	0.0525
A @ 0 mmHg	0.8938	0.7737	0.9471	0.9738	0.8404	0.9471
H/A @ 0 mmHg	0.0988	0.1263	0.0875	0.0788	0.1075	0.1013

Note: basal collagen 25% and elastin 7%. Wall thickness and internal diameters of the vessels are digitized data from Figure 3 in Nagasawa et al.[17]. The numbers shown are therefore estimations from the digitized image. The values are shown to four decimal places to portray the small relational differences between the values, not as an indication of accuracy.

Constriction of the artery begins on the second day after treatment and coincides with a drastic decrease in the collagen to elastin ratio (C:E). Both the collagen and elastin increase during the post SAH period, but the elastin has a much higher accumulation rate during the initial 2-day period than collagen. This causes the initial drop in the C:E ratio, but the value recovers somewhat by the 28th day. The maximum contraction is seen on day 7 in this study and on day 4 in a previous study conducted by Kuwayama et al.[7]. By the 28th day the diameter response returned to the control value. Consistent with the trends in the maximal constriction and C:E ratio, the incremental elastic modulus was found to significantly decrease on day 2 and recover gradually by day 28. The wall thickness to inner diameter ratio at 100 mmHg does not show any significant changes. The wall thickness to inner diameter ratio of 0 mmHg does show slight differences in values over the 28 days, as does the inner diameter at 0 mmHg.

Before a clear picture of vasospasm can be developed it is imperative to understand the complex interplay between the mechanical behavior, contractile response, structural components, and the chemo-mechanical signals. As vasospasm progresses, pressure-diameter curves shift leftward (Figure 3), reaching a maximal stiffness at the

peak of vasospasm then trending back toward 'Normal' behavior during recovery. Based on the current (albeit incomplete) understanding of vasospasm, we feel the condition must be examined as a growth and remodeling process. To rigorously interpret data in any growth and remodeling process, a thorough understanding of the 'normal' conditions is crucial. To date, the mechanics of the normal cerebral vasculature, and in particular that of common animal models, has not been well-characterized.

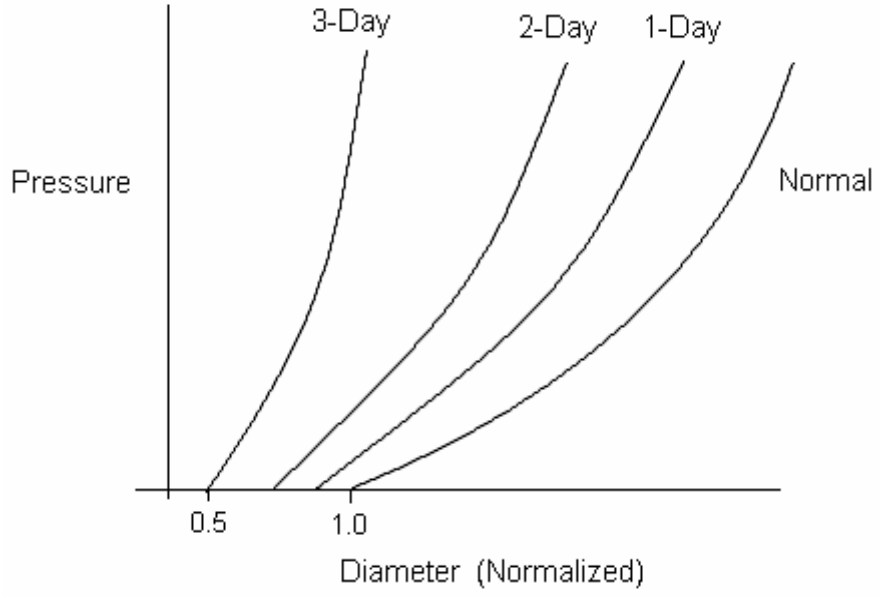

Fig. 3: Predicted mechanical behavior of vasospastic vessel. As vasospasm progresses, the vessel will increase in both stiffness and decrease in diameter. As the vessel moves to recovery the curve will shift back toward the normal curve[17].

Mechanics in the Normal Cerebral Vasculature

In two related publications, Hayashi et al.[19,20] evaluated the circumferential structural stiffness, β (Equation 1) and elastic properties, E_{inc} (Equation 2), of

cannulated whole arteries retrieved from autopsies. The intracranial vertebral and basilar arteries were tested as well as the extracranial vertebral, internal carotid, common carotid, and femoral arteries. Alterations in both structural stiffness and the elastic properties were evident between intracranial and extracranial arteries as well as 'young' and 'old' arteries. The intracranial arteries were generally stiffer than the extracranial arteries across all ages, with the one exception of the femoral arteries of a middle-aged person[19,20]. In addition to having significantly higher β values initially, the trend of increasing stiffness with age in intracranial arteries begins soon after birth. Extracranial arteries, however, have low β values at birth and significant increases in stiffness do not occur until after 40 years of age[19,20]. Intracranial arteries under 45 years of age also had a much higher E_{inc} than extracranial arteries. E_{inc} decreased with age in the intracranial arteries until it was similar to that of the extracranial arteries, which displayed no significant alterations across all ages. Intracranial arteries were also found to experience higher wall stresses in young arteries than old, the reduction of which in old arteries was suggested to be a result of an increase in the wall thickness to inner radius ratio.

Historically, mechanical studies of cerebral vessels have largely focused on the medial layer, ignoring the axial mechanical properties. In studies designed to investigate the axial mechanical properties of cerebral blood vessels, Monson et al.[25,26] performed axial static and dynamic failure testing on unpressurized, unperfused fresh human cerebral blood vessels. The cerebral arteries were found to be significantly stiffer, failing at much lower stretch values than extracranial arteries. As in the circumferential stress/strain relationships[19,20], the axial stress/strain response was exponential with an increasingly linear response at higher stretches until the point of yield and failure.

Intracranial arteries failed on average at a stretch of 1.4 and an axial stress of 3-5 MPa[25]. Cortical arteries specifically had a yield stretch of 1.38 and a yield stress of 3.6 MPa[26]. However, as the vessels were not tested in an in vivo geometry, the resulting failure values may not directly translate to the in vivo vessel characteristics.

To better interpret vasospasm experimentation, a more complete characterization of the normal cerebral vasculature is required. Ring tests can provide insight into some mechanical properties of arteries, however, it cannot be assumed to directly relate to the in vivo behavior as rings are not under axial stretch seen in vivo. Biaxial vessel response for vessels in physiologic conditions and orientations must be catalogued before the accurate interpretation of complex pathogeneses mechanisms. Of particular interest for vasospasm is the non-pathogenic axial and circumferential behavior of rabbit basilar arteries, a common SAH model.

Contractility in the Normal Cerebral Vasculature

The normal cerebral vasculature contractile response is multi-faceted. Not only is it tightly controlled by autoregulation mechanisms to prevent alterations in blood flow that would impair normal brain function; it responds to vasoactive molecules differently depending on method of application, concentration, transmural pressure and luminal flow conditions. High levels of potassium stimulate maximal contraction, shifting the pressure-diameter curves and ring length-tension curves to the left[19,22]. Dosing cerebral vessels with high levels of potassium (in the form of KCl) provides a good estimate of the contractile capability of the wall and can serve as an indicator of the viability of the functional capability of the smooth muscle cells[22].

Effects of pressure and flow on cerebral arterial response to KCl and 5-HT were evaluated by Vinall et al.[23] and Ohta et al.[24]. High potassium induced contraction was inversely sensitive to the transmural pressure, while 5-HT induced contraction showed no pressure dependence. Ohta et al.[24] verified the alterations in contractile response to extraluminally applied KCl due to variation of flow rate in pressurized and stretched rabbit basilar arteries. Serotonin contractions, though not pressure sensitive, did vary with method of application. At low concentrations (below 10^{-6} M) intraluminally applied 5-HT induced a stronger response than when applied extraluminally. KCl contraction is also dependent on application site. A 'transient phasic contraction' is seen when KCl is applied intraluminally, but extraluminal application results in only a 'rapid transient contraction'[24]. Cerebral areteries also are capable of generating intrinsic (myogenic) tone without application of vasoactive agents. Ohta et al.[24] confirmed basilar arteries spontaneously developed intrinsic tone when the flow rate was elevated above 10 ml/min. Vessel reactivity to mitogens and constrictors can also vary when multiple agents are present at one time, as is true in vasospasm.

Normal Cerebral Vasculature Microstructure

The normal vasculature structure has received much attention in recent literature, in part due to the need for information to motivate and improve mechanical models of vessel behavior. Cerebral arteries are muscular arteries with very low levels of elastin and no external elastic lamina[27]. The overall structure of cerebral arteries is divided into three layers: adventitia, media and intima. The adventitial layer is thought to be composed of collagen primarily in an axial orientation, though possibly also with a slight pitch[4]. In contrast, highly aligned circumferential collagen fibers and smooth muscle comprise the

media. The intima includes a thin subendothelial layer, a distinct internal elastic lamina and axially oriented endothelial cells[29]. Walmsley et al.[27] reported the basilar artery wall by percent composition as 15 ± 0.9% intima, 49 ± 5.6% media, and 36 ± 1.2% adventitia. The smooth muscle cells dominate the medial layer, comprising 69% by volume[27]. The edge of the smooth muscle layer marks the boundary between the media and the adventitia[29]. Generally cerebral vessels have higher C:E ratios when compared to extracranial arteries, a difference attributed to lower levels of elastin in cerebral arteries[19,20,21].

Collagen fibers are the primary load-bearing constituent in the wall. To evaluate collagen fiber contribution to the vessel's mechanical behavior several groups have investigated the orientation of adventitial collagen in human brain arteries at varying levels of transmural pressure. Canham et al.[37] suggested that although the adventitia had historically been dismissed as trivial for the mechanical function of the artery, it contributed significantly to the mechanical behavior particularly at and above physiologic pressures. The collagen in the adventitia would require a more thorough consideration in vascular mechanics if the circumferential collagen fiber component could be confirmed to adopt an 'increasingly coherent organization' with elevated transmural pressures. Canham et al.[37] utilized polarized light microscopy to evaluate the birefringence of collagen fibers in stained histological sections of cerebral arteries. With increasing pressure, the authors found a significant increase in the circumferential component of the adventitial collagen. However, the analysis of axially oriented fibers from traditional sections, as well as errors introduced by dehydration, pressure fixation, sectioning, and the unrecorded axial stretch make the extraction of meaningful fiber alignment

measurements difficult, if not impossible. Also, data from the outer layers of the adventitia also could not be analyzed.

Rowe et al.[29] also assessed the collagen orientation in cerebral arteries with the use of polarized light microscopy. Focusing mainly on the structural organization of the bifurcation region, the authors pressure fixed middle cerebral, basilar, posterior cerebral, and posterior communicating arteries. Analysis of the birefringence of the collagen in the sections and prior orientation measurements[31] led the authors to estimate the adventitial collagen to contribute to 1/3 of the circumferential strength and all of the axial strength of the arteries. Similar potential errors as Canham et al.[37] were noted.

To better assess the axial orientation of collagen fibers in the adventitia, Finlay et al.[31] utilized a tangential sectioning procedure prior to analysis with polarized light microscopy. Mean fiber orientations for the adventitia and media of autopsied human cerebral arteries were quantified at three pressures: 30, 120, and 200 mmHg. The authors found medial collagen to have a highly aligned circumferential orientation and adventitial collagen with a wider distribution about a mean axial orientation. However, the vessel preparation techniques (paraffin embedding and sectioning) as well as no controlled axial stretch could introduce error in the angle quantification.

The current methods of structural analysis do not allow for capture of collagen fiber orientation of live, intact arteries in in vivo geometries, introducing complications and analysis. To date a precise descriptor of fiber distribution and orientation in all layers of cerebral arteries has not been catalogued, hindering the development of structurally-based models of mechanical behavior.

The work presented here will address several aspects of the mechanical and structural properties of the normal cerebral vasculature, specifically that of the rabbit basilar artery, that have not been fully characterized. Biaxial testing and the resulting stress-stretch curves will outline properties for acute and short-term culture rabbit basilar arteries. Maximally-contracted artery testing will provide a framework for interpreting vessel basal tone and alterations in contractile capability. Quantifying collagen fiber orientation as a function of radius will support the development of accurate mathematical models connecting mechanical behavior and microstructural elements.

METHODS

Using a custom ex vivo organ culture and mechanical testing device, acute and cultured basilar arteries from male White New Zealand Specific Pathogen Free (SPF) rabbits underwent cyclic pressurization tests at in vivo conditions and controlled levels of smooth muscle tone. Sections of basilar arteries were also imaged for transmural collagen fiber orientation at 0, 40 and 80 mmHg at in vivo stretch conditions using nonlinear optical microscopy (NLOM). Combined mechanical and structural data allowed current stress-strain relations for arteries to be assessed more completely than previously possible.

Device

In order to control the chemical and mechanical environment, testing and culture was carried out in a modified version of a 'multiaxial computer-controlled organ culture and biomechanical device'[8] (Figure 4). This organ culture device allows concurrent biaxial mechanical testing and culture while small blood vessels are maintained in a physiologic geometry and environment. The vessel culture chamber isolated the artery in a sterile environment while still allowing the movement necessary for mechanical testing (Figure 5).

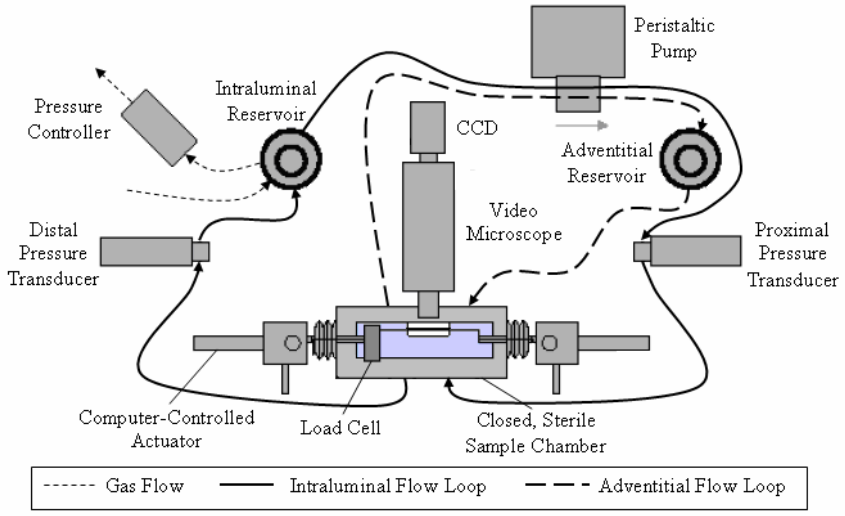

Fig. 4. Schema of the modified multiaxial computer-controlled organ culture and biomechanical device.

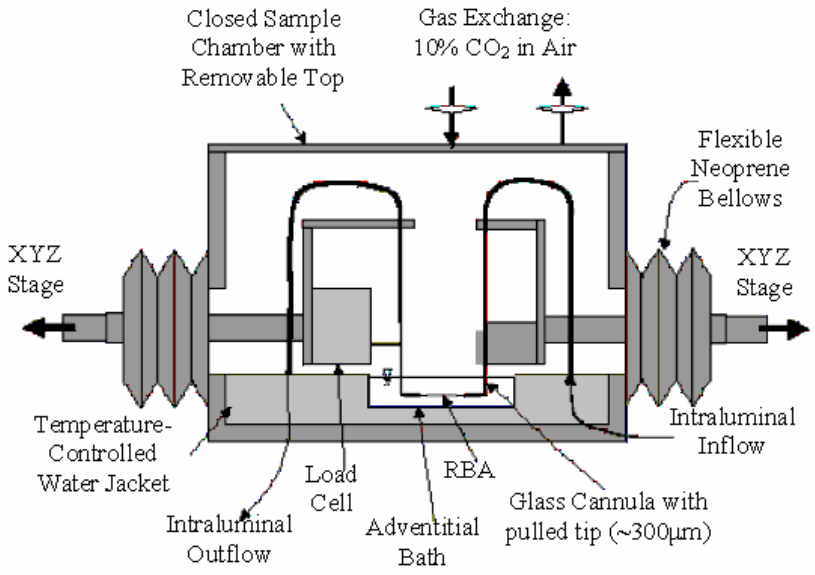

Fig. 5. Close-up schema of the culture chamber. RBA denotes rabbit basilar artery.

Vessel Extraction and Preparation

Within a laminar flow hood, the rabbit basilar artery was extracted from the base of the skull with the surrounding brain tissue and spinal cord. The artery was then

removed from the brain stem and cleaned under a microscope. The basilar artery was divided into two equal sections (~5-6 mm length); the upper portion designated for imaging and the lower portion for mechanical testing. Following ligation of the larger branches in the lower portion of the basilar with sterile 7-0 suture, the artery was secured using 6-0 ligatures onto custom glass cannula (~300 μm tip) in the in vitro testing device. The system was then sealed to protect against contamination. In order to stabilize and control the intraluminal pressure, the numerous remaining small branches were occluded via an injection of dextran microspheres (133 to 215 μm in diameter, Cytodex 3, Sigma) into the lumen. Microspheres, when injected while the artery is pressurized, move into the unligated branches and prevent vessel leakage (black arrows, Figure 6).

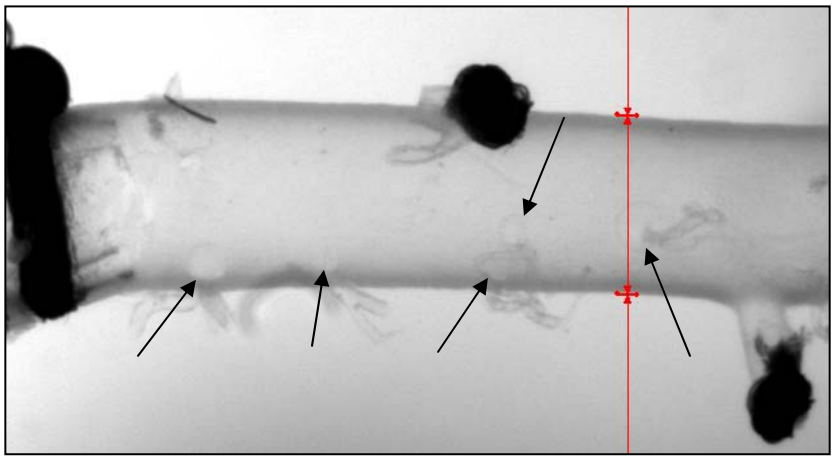

Fig. 6. Image of a rabbit basilar artery at 7 mmHg captured with a Video Microscope/CCD. Note the suture on the left holding the vessel onto the glass cannula tip, the ligated branches, the red lines marking the outer diameter, and the microspheres occluding the unligated branches. The black arrows point to the microspheres.

Mechanical Testing Protocol

Once the pressure was stabilized and system setup completed, the unloaded length of the artery and diameter were measured and recorded. 'Unloaded' conditions were set

at a transmural pressure of 7 mmHg; pressures less than 7 mmHg did not consistently prevent collapse. The unloaded length was denoted as an axial stretch of 1.0 (0% extension from the unloaded length). From preliminary pressure-axial force data on the rabbit basilar artery, the in vivo stretch was estimated to be 1.15 (15% extension from the unloaded length) according to the method of van Loon et al.[39]. A conservative estimate of the in vivo transluminal blood pressure in the rabbit basilar is 80 mmHg, that is, the difference between a mean arterial pressure of 85 mmHg and a cerebrospinal fluid pressure of 5 mmHg. Following an acclimation period of 30 minutes, the artery underwent a gradual preconditioning process (three cycles at 1.1 stretch: 7-60 mmHg, 7-70 mmHg, 7-80 mmHg; three cycles at 1.2 stretch: 7-70 mmHg, 7-80 mmHg, 7-80 mmHg) to protect against damage of the tissue during testing and to minimize hysteresis. Wall thickness measurements were taken from the preconditioned vessel at lengths of 1.1, 1.15, 1.2 and pressures of 7, 40, and 80 mmHg, which invoking the incompressibility assumption allows wall thickness to be estimated during cyclic tests based on measurements of one radius and the axial stretch. The unloaded length and diameters were measured and recorded again following preconditioning. The mechanical testing protocol consisted of cyclic pressure-fixed stretch tests at stretches of 1.1, 1.15, 1.2 and pressures cycling from 7-80 mmHg. Pressure-diameter data were recorded along with axial forces. The pressure was never lowered to 0 mmHg to prevent the microspheres from dislodging from the branches. Our stretches of 1.1, 1.15 and 1.2 are also well below the axial yield and failure values of 1.4 reported by Monson et al.[25,26].

Viability Testing

To determine the viability of the basilar artery, a 60mM KCl solution was injected into the adventitial bath and the decrease in diameter was measured over 15 minutes. A contraction of 30% was considered a fully 'viable' artery. While maximally contracted in the KCl solution, another cyclic pressure-fixed stretch testing protocol was executed on a subset of arteries to record the artery behavior under high levels of smooth muscle tone. KCl was chosen for the viability testing because it has been verified to have a reversible response and is an indicator of both contractile capacity and smooth muscle cell viability[22]. Following active testing, the KCl solution was washed out of the adventitial bath three times with sterile saline prior to refilling the bath with the proper culture media mixture. Once vessel relaxation to the pre-active testing diameter was verified, the culture chamber was removed from the mechanical testing device and moved to an incubator.

Culture Conditions

While in the incubator, the basilar artery was subjected to physiologic pressure and flow conditions. The following conditions were used to mimic the in vivo environment for a rabbit basilar artery: 80±5 mmHg intraluminal pressure, 1.15 axial stretch, 6 mL/min flow (2 Pa wall shear stress), 37° C temperature, 10% CO_2. The culture media consisted of Advanced DMEM (Invitrogen), 1% Penicillin/Streptomycin (Invitrogen), and 1% Fetal Bovine Serum (Atlas Biologicals). The culture chamber was removed from the incubator and re-connected to the mechanical testing device on days 1 and 2 of culture. The associated mechanical and viability testing followed the above protocols with one exception: the artery did not undergo the initial preconditioning phase. Preconditioning was deemed unnecessary considering the vessel was kept at estimated in

vivo conditions throughout culture and re-connection time to the mechanical testing device was modest (~5 minutes).

Imaging

A nonlinear optical microscopy (NLOM) system is capable of imaging structural components throughout the thickness of a blood vessel wall while the vessel remains alive and intact[30,32]. Second harmonic generation (SHG) was used to image the fibrillar collagen fibers in the adventitia and media in 1 micron steps through the thickness of the wall[32] (Figure 7). Prior to imaging, the lower half of the basilar artery was also cleaned, ligated, and cannulated in a custom imaging chamber**.** Using the imaging chamber, it was possible to stretch, perfuse, and pressurize the artery while allowing the NLOM system to be within the range for proper imaging. Pressure stabilization by ligation and microsphere injection was implemented for imaging to ascertain fiber direction information under physiologic pressure conditions (80 mmHg). The stretch of the artery also affects the undulation of the collagen and the subsequent determination of fiber orientations, thus the artery was stretched to the approximate in vivo condition of 1.15. For comparison, the basilar was also imaged at 0 and 40 mmHg at the in vivo stretch.

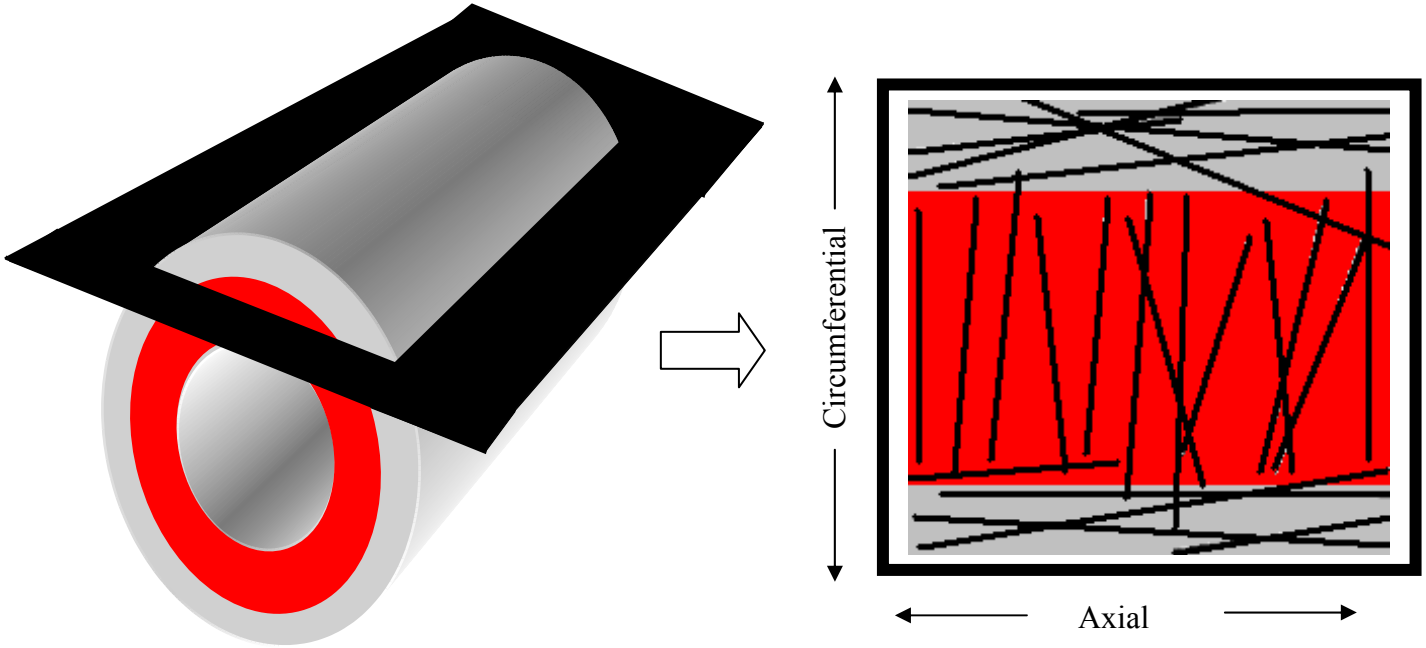

Fig. 7. Schematic drawing of an optical slice (1 μm thick) obtained with NLOM second harmonic generation. On the left the adventitia is solid gray, the media is red, and the optical slice is black. Note that the curvature of the vessel can capture collagen in the adventitia and media within a single optical slice (right, medial section boxed in red dashed line, adventitial section boxed in gray dotted line). This motivates a cropping of the images prior to analysis to minimize the effects of curvature.

Data Analysis

Since a direct optical measurement of the inner radius is difficult to obtain automatically, the inner and outer radii were manually marked and measured at three lengths and multiple pressures using the image capture setup and LabView software[8]. This thickness data were used to calculate the deformed inner radius, a, using Equations (9) and (10) and the assumption of incompressibility. Each recorded inner and outer radius was used to calculate a volume for the artery using Equation (9) where b is the outer radius, $\hat{a}$ is the inner radius, l is the length, and V is the volume of the artery. These volumes were averaged, $\overline{V}$, and used in Equation (10) for inner radius calculations at any other condition, a.

$$V = \pi(b^2 - \hat{a}^2)l \qquad (9)$$

$$a = \sqrt{b^2 - \overline{V}/(\pi l)} \qquad (10)$$

Equations (9) and (10), along with pressure-diameter-axial force data recorded during testing were used to calculate the circumferential Cauchy stress and stretch. Equations (11), (12, 13) are the mean circumferential stress and stretch, respectively, where P is the transmural pressure, a is the inner radius, h is the wall thickness, and σ_θ is the mean circumferential stress.

$$\sigma_\theta = \frac{Pa}{h} \qquad (11)$$

$$\lambda_\theta^* = \frac{(a+b)/2}{(A(0)+B(0))/2} \qquad (12)$$

$$\lambda_\theta = \frac{(a+b)/2}{(A(s)+B(s))/2} \qquad (13)$$

λ_θ^* is the circumferential strain with respect to the unloaded inner and outer diameters on day 0, $A(0)$ and $B(0)$; and λ_θ is the circumferential strain with respect to the unloaded inner and outer diameters on the day of testing, $A(s)$ and $B(s)$. The resulting stress-strain curves were then used to identify, via nonlinear regression, values of the material and structural parameters in a four-fiber family model[12].

Equation 14 is the strain energy function for a four fiber family Holzapfel-type model of the passive behavior.

$$W = \frac{c}{2}(I_1 - 2) + \sum_{k=1,2,3,4} \frac{c_1^k}{4c_2^k}\left\{\exp\left[c_2^k\left(\left(\lambda^k\right)^2 - 1\right)^2\right] - 1\right\} \quad (14)$$

Note that I_1 is the first invariant of the right Cauchy-Green tensor and c is an associated material parameter; this term models the assumed isotropic contribution of the elastin. Fiber families 1 and 2 are oriented diagonally, while family 3 is axial (0°) and family 4 is circumferential (90°); these model predominantly the collagen fibers but the circumferentially oriented family can also model passive smooth muscle – see Figure 8. The superscript *k* denotes the k^{th} fiber family and c_1^k, and c_2^k are the material parameters for the fiber families. For convenience, we let the material parameters for the diagonal fibers be equal, $c_1^1 = c_1^2$ and $c_2^1 = c_2^2$, and similarly for the parameters associated with the axial and circumferential fibers, $c_1^3 = c_1^4$ and $c_2^3 = c_2^4$ (cf. Hu et al.[12]). Finally, λ^k is the stretch of the k^{th} fiber family (Equation 15), which is calculated as

$$\lambda^k = \sqrt{\lambda_\theta^2 \sin^2\alpha^k + \lambda_z^2 \cos^2\alpha^k} \quad (15)$$

where α^k represents the angle between the diagonal fiber family and the axial direction. Note, for example, that one could also have $\alpha^3 = 0°$, $\alpha^4 = 90°$, which yields the axial and circumferential stretches for these families as expected.

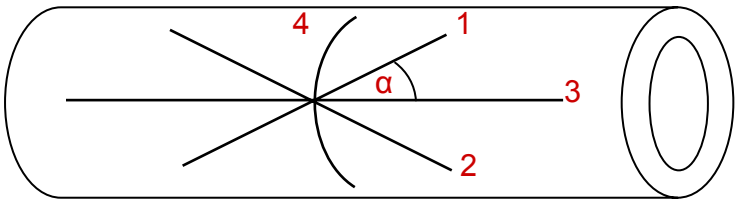

Fig. 8. Illustration of the four fiber family Holzapfel-type model. Families 1 and 2 are oriented diagonally, while family 3 is axial (0°) and family 4 is circumferential (90°).

Best-fit values of the material and structural parameters can be determined using nonlinear regression and the minimization of an objective function e that accounts for differences between theoretically predicted and experimentally measured values, namely,

$$e = \sum_{i=1}^{N} \left[\left(\frac{P^{Theory} - P^{Exp}}{P^{Exp}} \right)_i^2 + \left(\frac{F^{Theory} - F^{Exp}}{F^{Exp}} \right)_i^2 \right] \quad (16)$$

The superscript 'Theory' denotes the variable calculated using Equations 11-15 whereas the superscript 'Exp' denotes the experimental data, with N the number of data points. Using Matlab, the experimental data were fit using the fminsearchbnd function with six parameters, $c_1^{1,2}, c_2^{1,2}, c_1^{3,4}, c_2^{3,4}$, c, α. All parameters had a lower bound of 0, but only α was bounded above by 90.

All imaging data were processed using ImageJ (available vis the NIH), Continuity (available from Prof. A McCulloch, UCSD), and Matlab. The curvature of the vessels and the flat optical imaging necessitated cropping of the images to reduce error in

interpretation. All images were cropped in ImageJ to at most 200 microns in the direction perpendicular to the axial direction. Continuity imports TIF images and outputs fiber markings (Figure 9, left) and fiber orientations (Figure 9, right) in a tab delimited spreadsheet. For each imaged slice through the wall, collagen fiber orientation was compiled in Matlab and fit with a probability distribution in Microsoft Excel. The fiber orientations obtained from imaging were then compared to those predicted using the four-fiber family model.

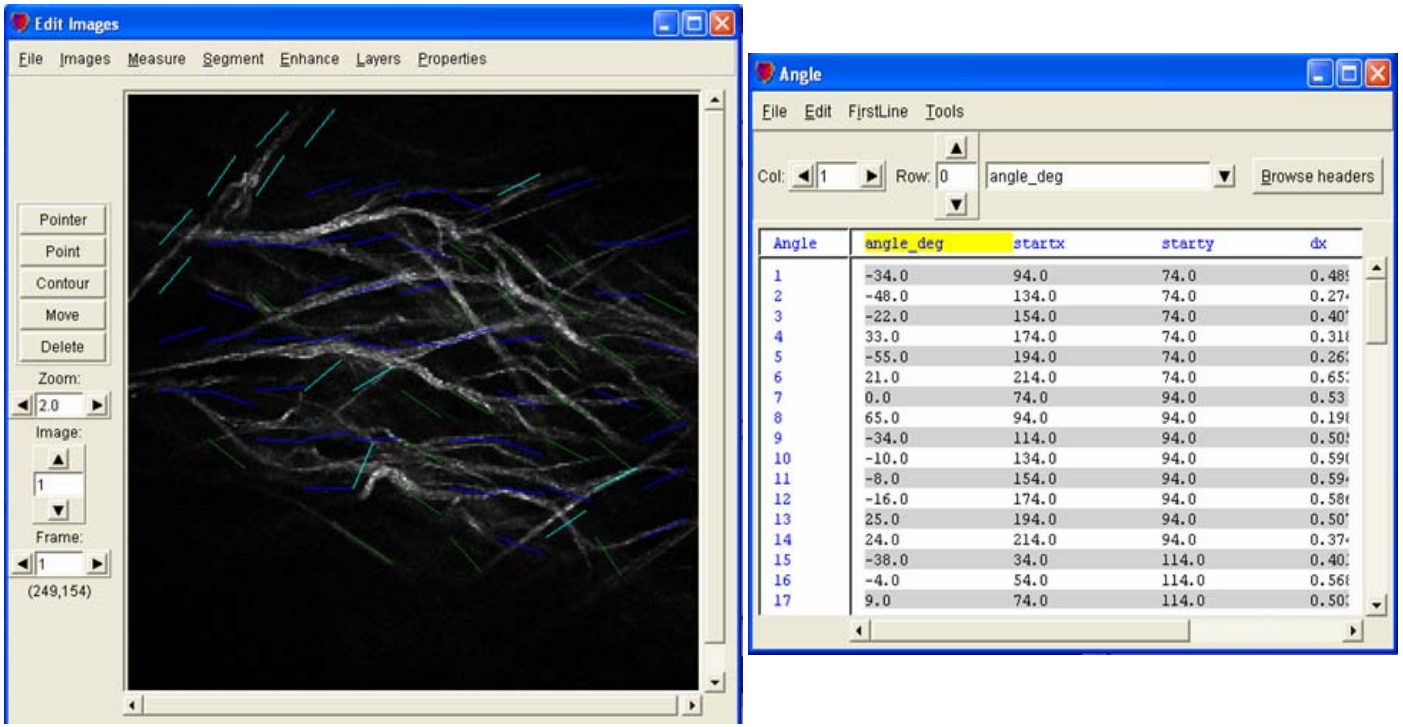

Fig. 9. Menus in the image processing portion of the code Continuity. Continuity inputs optical slices and outputs visual fiber markings (left) and numerical fiber orientations (right). In particular, blue markers indicate orientations in the range of -25° to 25°, green markers -25° to -70°, cyan markers 20° to 70°, and red markers (not represented in figure) 70° to 90° and -70° to -90°.

RESULTS

Mechanical Data

Pressure-diameter and circumferential stress-strain curves of mean data from 6 vessels at an axial stretch of 1.15 show the expected nonlinear response (Figure 10). Diameter was normalized using data from the unloaded state, which eliminated variations in vessel diameter and thus allowed data to be averaged and compared directly. Pressure-diameter, axial force-pressure, and circumferential stress-strain graphs were used for visual assessment (Figures 10-13).

Potassium chloride activation of the smooth muscle cells caused the active curve to shift leftward with the appearance of a flexion point around 15 mmHg (Figure 11). At higher pressures the active and passive curves had similar shapes and slopes. Characteristic data from active / passive experiments are shown in Figure 11.

Data associated with all three stretches (1.1, 1.15, and 1.2) are plotted together for comparison (Figure 12). As expected, increased axial stretch tended to stiffen the vessel circumferentially as revealed by the curves shifting to the left.

When cultured at in vivo conditions, Day 0, 2 specimens have nearly identical pressure-diameter and circumferential stress-strain curves (Figure 13). The vessel on Day 2 also met the viability criteria, exhibiting a 30% constriction in response to KCl.

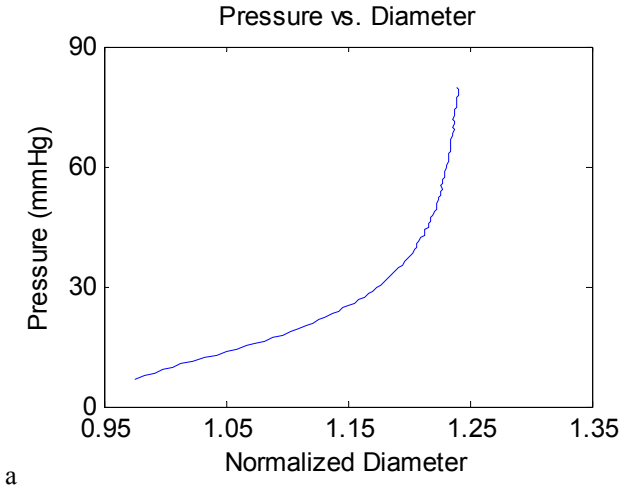

a

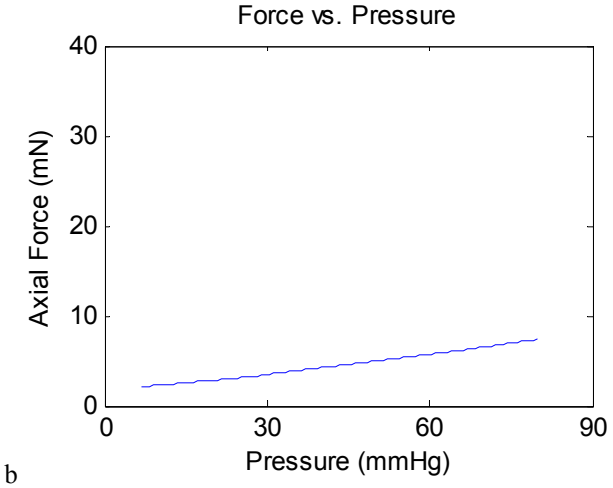

b

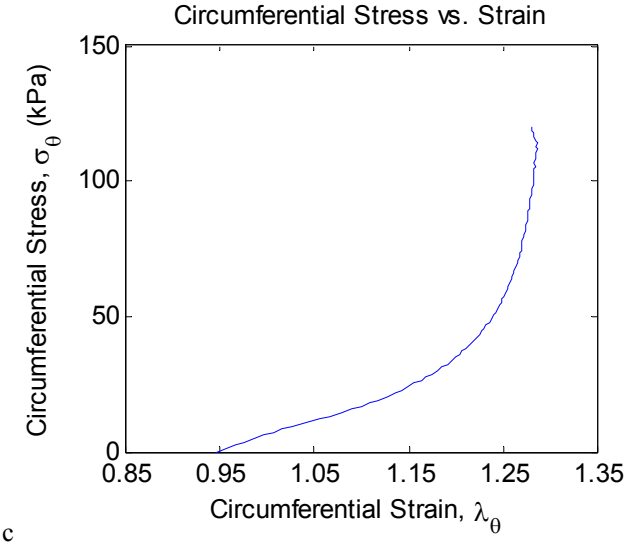

c

Fig. 10. Mean pressure-diameter, axial force-pressure, and circumferential stress-strain plots (N=6). (a) Pressure and diameter curve at in vivo stretch ($\lambda_z = 1.15$). Diameter is normalized using data from the unloaded state. As pressure reaches physiologic values the vessel distends less, which can be seen in the increasing slope. The data displays the expected nonlinear response. (b) Force and pressure data averaged from 6 sets. (c) Circumferential stress and strain data. The data displays the expected nonlinear response.

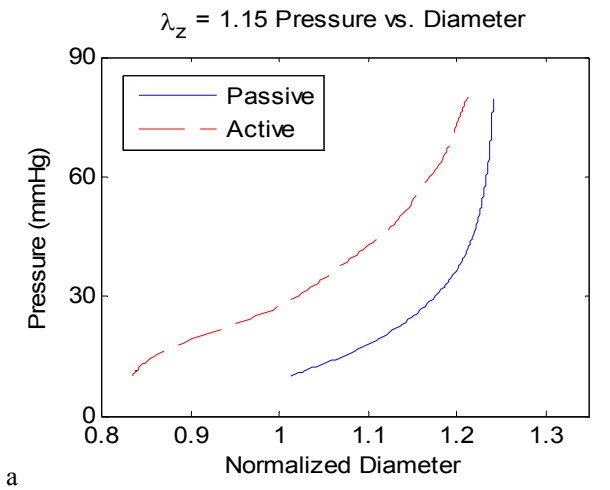

a

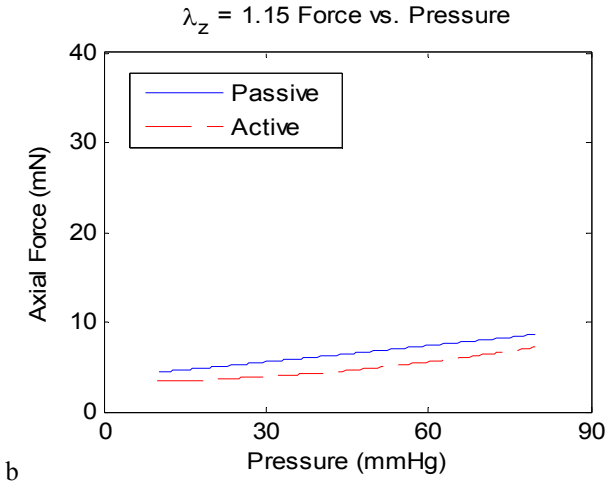

b

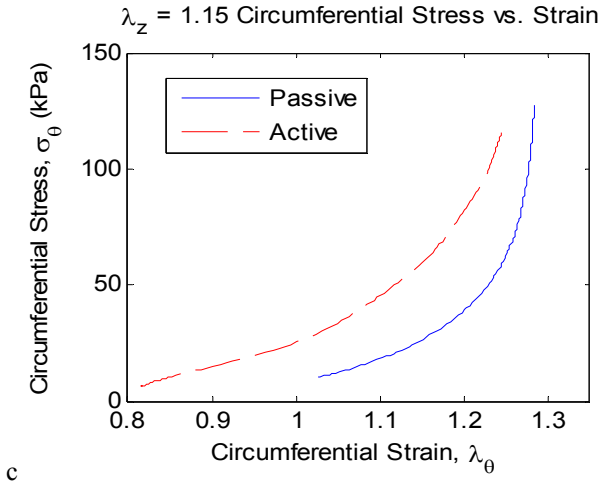

c

Fig. 11. Characteristic data from active/passive experiments. (a) Active and passive pressure diameter curves at 1.15 stretch. At lower pressures the active curve is shifted to left and a flexion point can be seen around 15 mmHg. As the pressure increases the active curve gets closer to passive curve and begins to have a similar shape. (b)Active and passive force-pressure data at 1.15 stretch. Less axial force is generated by the active vessel than the passive vessel at increasing pressures. (c) Active and passive circumferential stress and strain data at 1.15 stretch. At lower pressures the active curve is shifted to left of the passive curve, but a flexion point is not clearly visible. As the pressure increases the active curve gets closer to passive curve and begins to have a similar shape and slope.

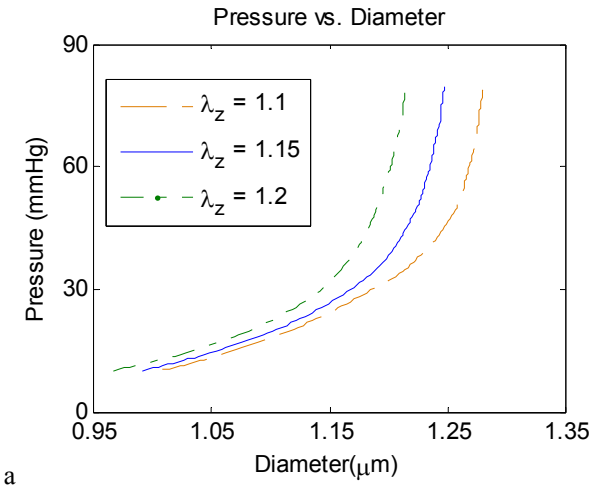

a

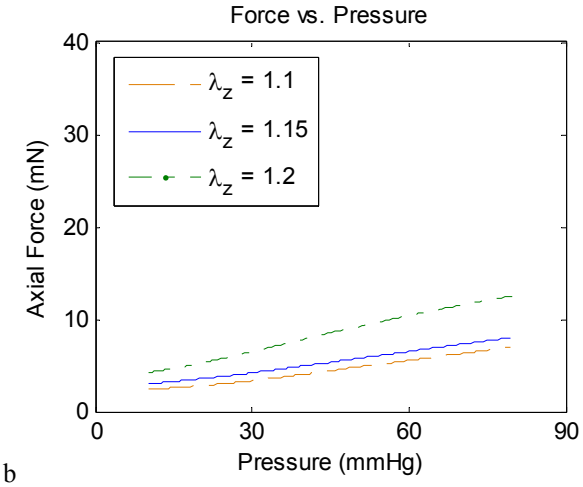

b

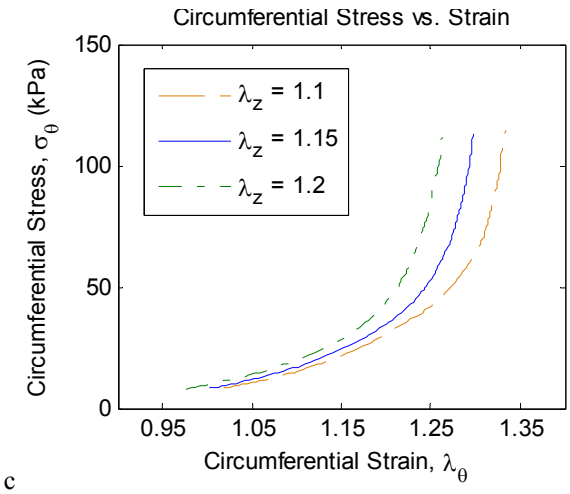

c

Fig. 12. Characteristic pressure-diameter, axial force-pressure, and circumferential stress-strain plots at three stretches (1.1, 1.15, 1.2). (a)Pressure diameter data. As the stretch increases the curve shifts to the left. (b)Axial force-pressure data. The stretch of 1.2 has an increasing slope showing a slight over stretch. The stretches of 1.15 and 1.1 have nearly identical slopes; however we choose to use a stretch of 1.15 due to the vessels tendency to bend at higher pressures at a 1.1 stretch. (c)Circumferential stress-strain data. As the stretch increases the curve shifts to the left. The curves near at lower stresses, but diverge at higher stresses.

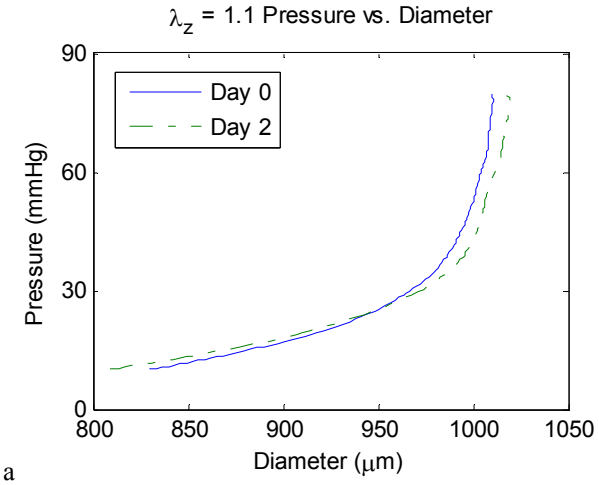

a

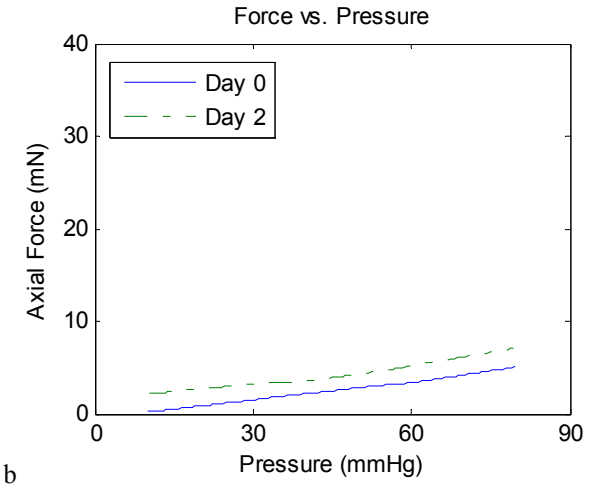

b

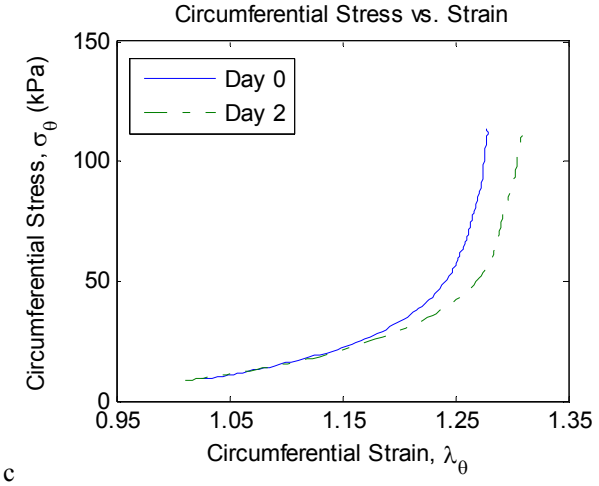

c

Fig. 13. Preliminary culture data. (a)Pressure diameter curves of preliminary culture data. Day 0 and 2 are very similar showing that mechanical properties can be maintained in ex vivo culture. (b)Force pressure from preliminary culture data. Both days have similar slopes. Unloaded length changed from 6.1mm to 6.3mm from day 0 to 3. (c)Circumferential stress strain curves from preliminary culture data. Day 0 and 2 show similar shapes showing that mechanical properties can be maintained in ex vivo culture.

Imaging

Illustrative optical slices from the same vessel at three pressures and an axial extension of 15% display the decrease in collagen undulation as the pressure increases (Figure 14). Images are oriented so the horizontal and vertical directions correspond to axial and circumferential orientations, respectively. Images (a) through (e) at each of the three pressures represent the splay from adventitia to media. Image (d) at all three pressures depicts a dramatic switchover from axially oriented fibers to circumferentially oriented fibers. The black spaces between the circumferentially oriented fibers in images (d) and (e) suggest the positions of smooth muscle cells, which cannot be imaged with SHG. Note the almost undetectable undulation of collagen fibers at a transmural pressure of 80 mmHg. Images (d) and (e) also motivate the image cropping during processing and analysis. Note the vertical center of the images progress to the medial layer faster than the top and bottom as a result of the vessel curvature in the circumferential direction.

Cropped imaging data for 6 basilar arteries at 80 mmHg and 1.15 stretch were normalized for comparison and compiled. To normalize the data and provide a meaningful comparison of fiber distribution between optical slices, fiber angles in each optical slice were calculated and divided by the total number of angles marked by Continuity within that slice. The resulting values represent the percent of fibers in that slice at that angle, but do not correlate to mass fraction of collagen. Corresponding slices in each of the six vessels were averaged together and plotted in a three dimensional histogram (Figure 15). The normalized position through the wall (0 to 1) indicates positions from the outer adventitia (0, and dark blue) to the inner media (1, and bright red). Constituents in the intima, such as the internal elastic lamina and basement

membrane, cannot be imaged using SHG and thus are not represented. The fibers in the adventitial region are distributed primarily around the axial direction (0°), whereas the fibers in the media are oriented nearly circumferentially (±90°). Characteristic slices from the adventitial and medial regions (Figures 16 and 17) display the stark differences in collagen orientation between the two layers. Each layer in the averaged 3D histogram was fit individually with a probability distribution. As the medial slices were bimodal in nature (±90°), and thus difficult to fit with a standard probability distribution function, the negative angles in these slices were changed to positive with the addition of 180°. A normal distribution was chosen for the adventitial layers (Figure 18) and a Student's t distribution was used for the medial layers (Figure 19). Figure 20 shows mean values for each slice. For comparison with 'helical angles' in the literature[31], seven characteristic optical slices were chosen from the adventitial region and the angles in each slice between 0° and 90° were averaged, resulting in a value of 19.8°. For comparison with model-calculated values of alpha (cf. Equation 15), all angles from the averaged data were averaged without angles from -85° to -90°, 85° to 90°, and -5° to 5° (which corresponds to the circumferential and axial fiber families), resulting in a value of 43.6°. The average including all angles was 44.9°.

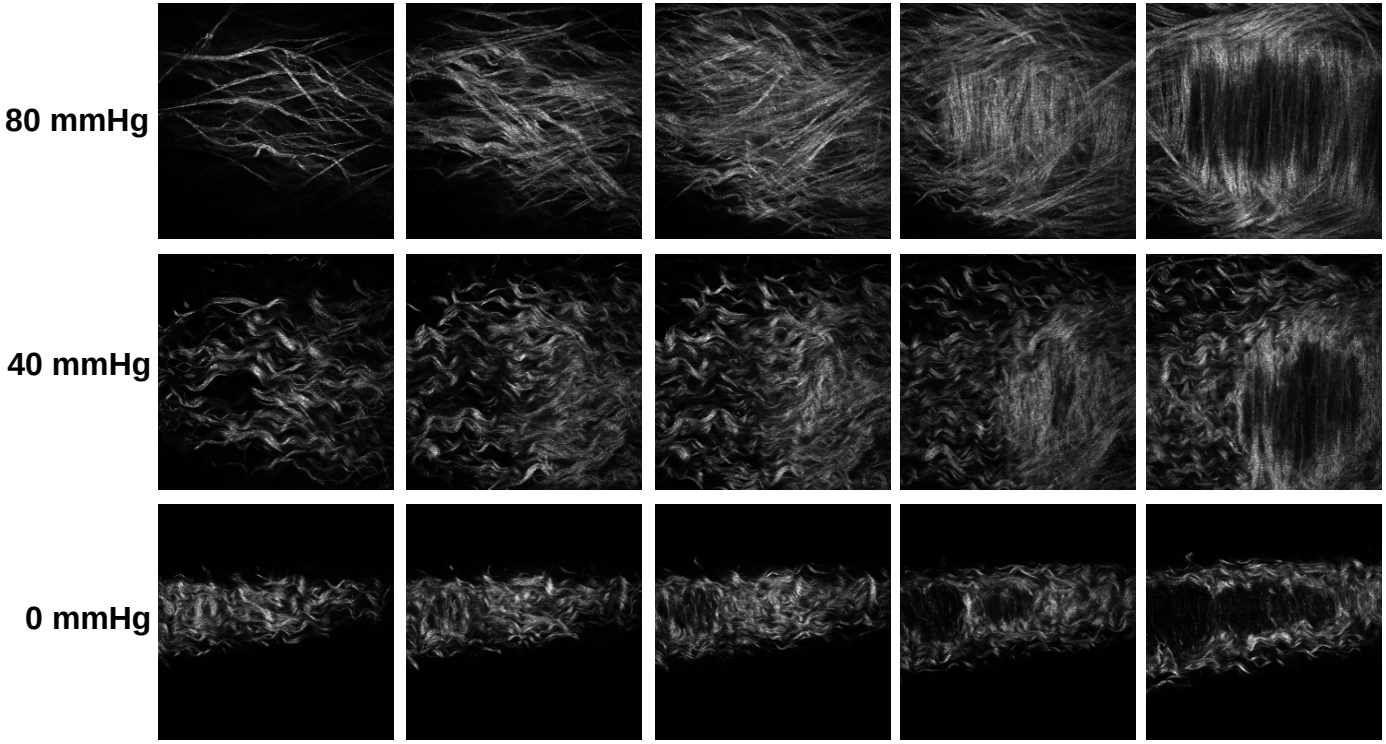

Fig. 14. Second harmonic generation (SHG) optical slices (uncropped) of a representative basilar artery held at 15% extension and imaged at 0, 40 and 80 mmHg. Images (a) through (e) for each pressure represent a sampling of slices from the adventitia to the media (too many slices to show each step). The images are oriented so that the horizontal direction is the axial direction of the artery and the vertical direction is the circumferential direction of the artery. In particular, note: the increased undulation with decreased pressure; the black 'holes' in the media, which are the smooth muscle cells; and the dramatic shift from axial to circumferential fibers. Finally, note the need for image cropping to get a more consistent measurement of fibers within the same layer.

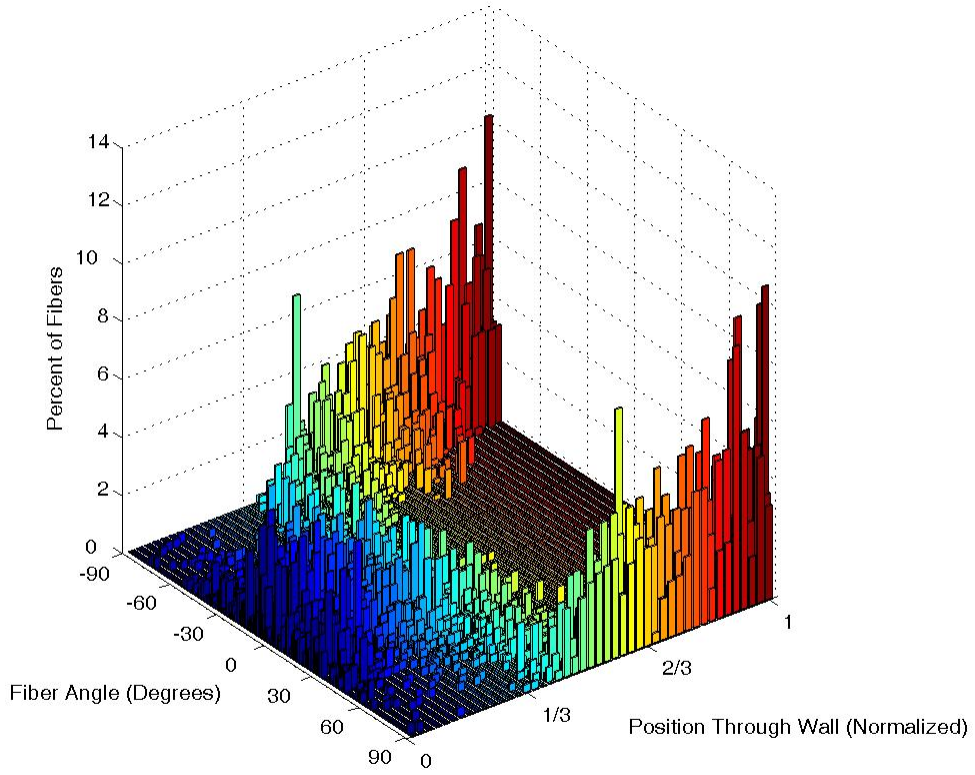

Fig. 15. Three dimensional histogram of normalized and averaged data sets (N=6) at 15% axial extension and 80 mmHg. The 'Position Through Wall' begins with 0 (blue), marking the outer adventitia, and ends with 1 (red), marking the inner media. Note: Constituents in the intima were not captured with second harmonic generation and are not represented. The 'Fiber Angle' axis is oriented so that 0° is axial and ± 90° is circumferential. Note the relative heights of the columns in respective layers do not correlate to fractional composition of collagen at that slice. For example, the higher columns in the medial layer slices seem to suggest the presence of higher levels of collagen in this layer, however, the opposite is true.

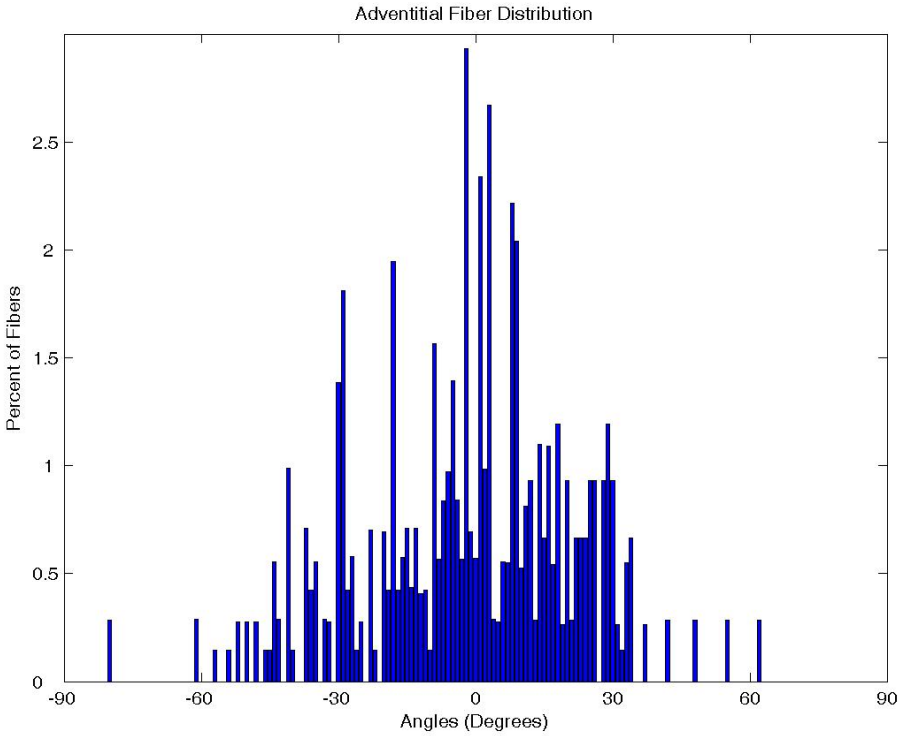

Fig. 16. A characteristic slice from the adventitial layer of the three dimensional histogram (Figure 15). The 'Angles' axis is oriented so that 0° corresponds to the axial direction and ± 90° is the circumferential direction.

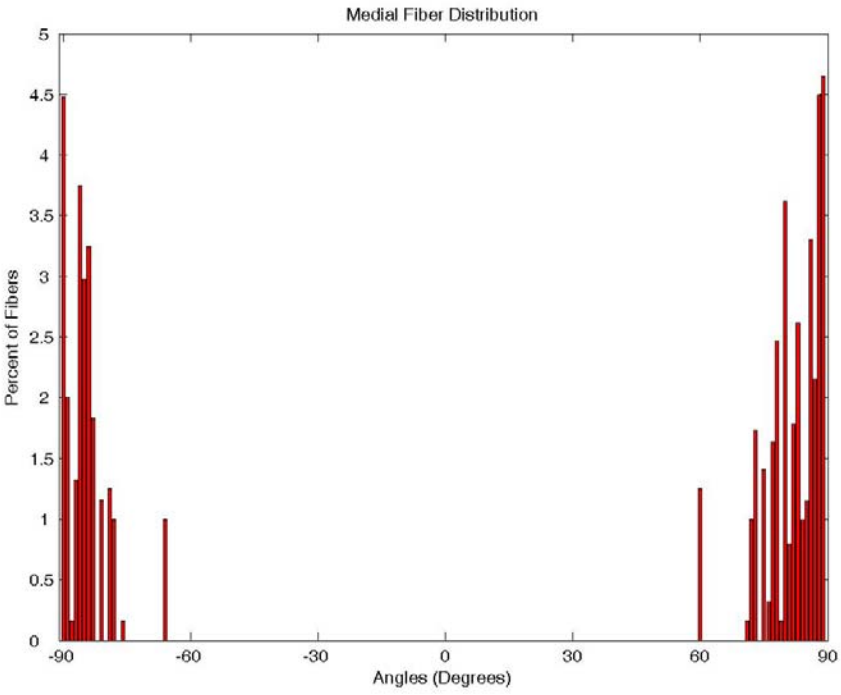

Fig.17. A characteristic slice from the medial layer of the three dimensional histogram (Figure 15). The 'Angles' axis is oriented so that 0° is the axial direction and ±90° is the circumferential direction.

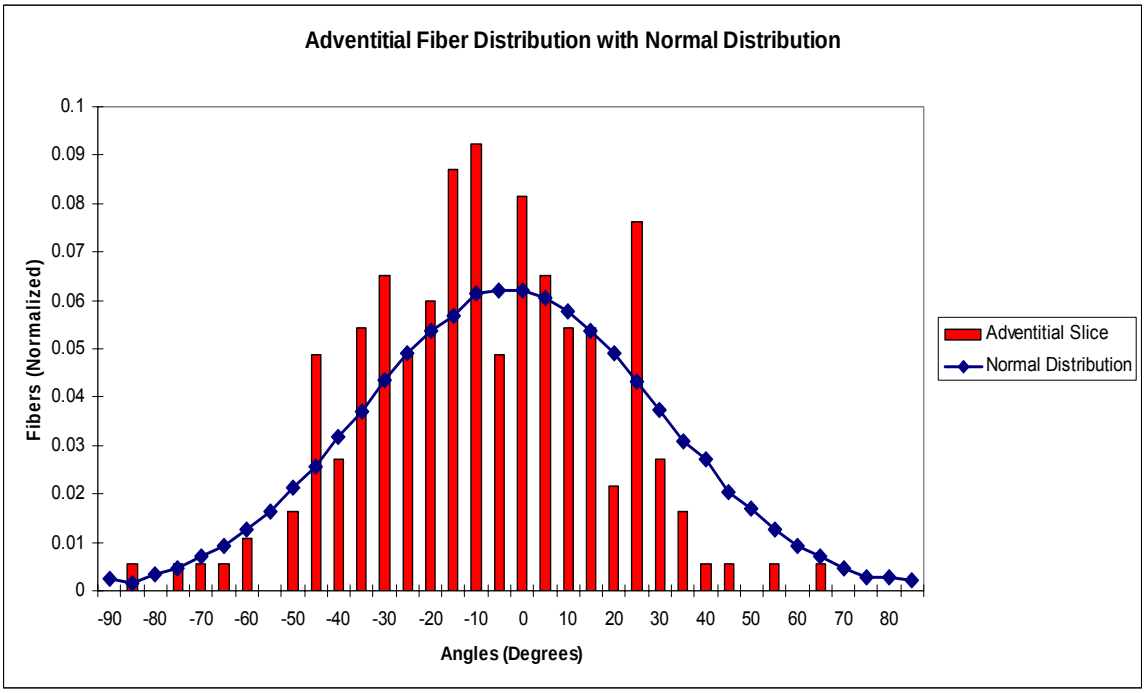

Fig. 18. Characteristic normal distribution fit on an adventitial slice. The normal distribution was chosen as an appropriate approximation across all optical slices in the adventitia.

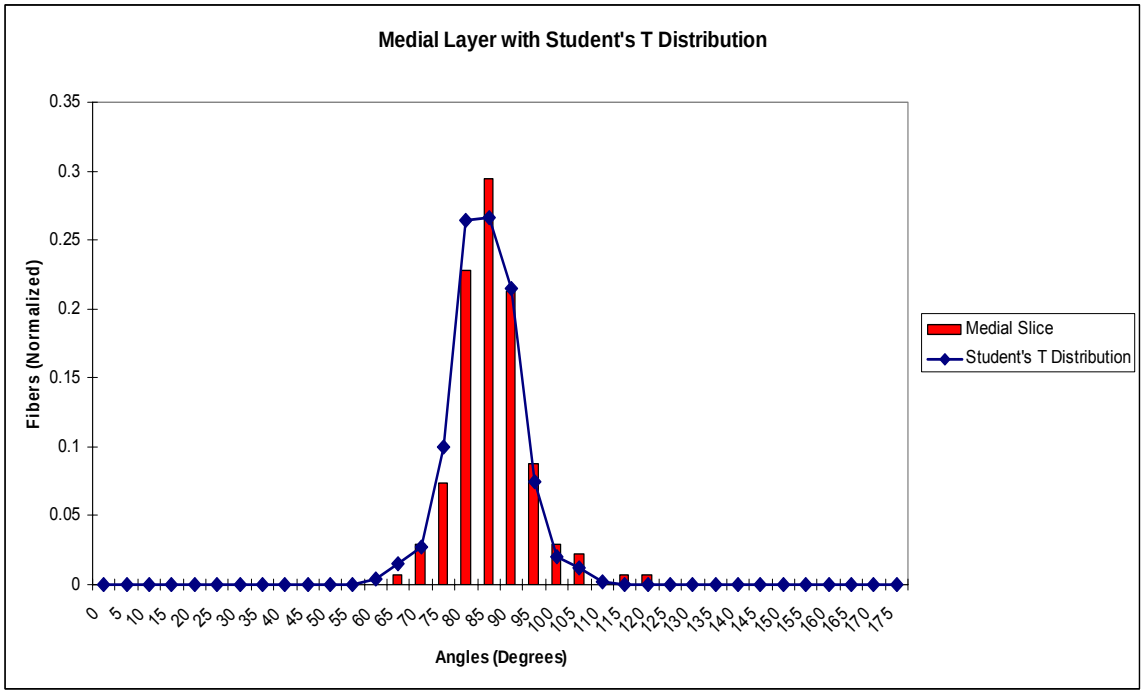

Fig. 19. Characteristic student's t distribution fit on a medial slice with modified angles. The student's t distribution was chosen as an appropriate approximation across all optical slices in the media. The 'Angles' axis is oriented so that 0° and 180° correspond to the axial direction and 90° is the circumferential direction.

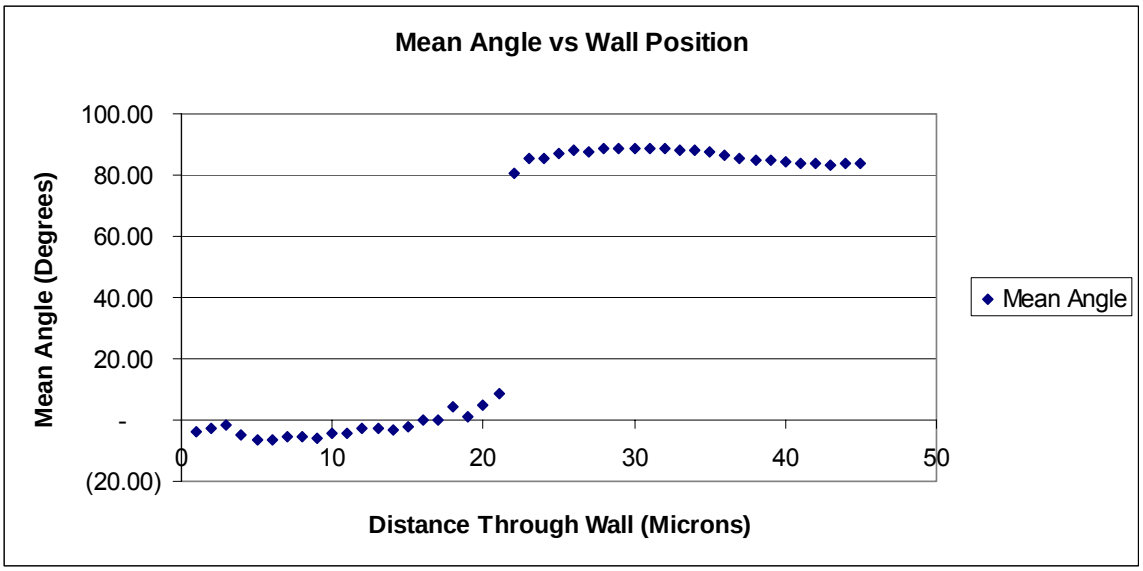

Fig. 20. Mean angle as a function of distance through the wall. 1 on the x axis corresponds to 1 micron depth into the wall from the outside of the adventitia. 0 corresponds to the outer adventitia and 45 corresponds to the inner media. The 'Mean Angle' axis is oriented so that 0° is the axial direction and 90° is the circumferential direction.

Model Fitting

Best-fit parameters (cf. Equations 14, 15) for the four fiber family model can be found in Table 2. Curves were then calculated using the parameters from the data fitting and plotted alongside the raw data (Figure 21).

Table 2. Best-fit material parameters for the 4-fiber Holzapfel-type model with mean and standard deviation of each parameter listed below.

Specimen	Material Parameters					
	c(kPa)	$c_1^{1,2}$ (kPa)	$c_2^{1,2}$	$c_1^{3,4}$ (kPa)	$c_2^{3,4}$	α (degrees)
1	4.56E-08	27.19	13.96	56.27	9.86E-04	40.83
2	7.27E-08	30.82	12.85	38.11	1.08E-03	42.10
3	6.34E-08	21.53	15.49	73.71	3.54E-04	38.76
4	1.16E-07	15.85	15.78	32.05	1.11E-03	44.86
5	2.32E-07	16.06	26.01	24.92	6.41E-04	48.17
6	1.18E-07	19.79	21.32	12.29	1.32E-03	47.15
AVE	1.08E-07	21.87	17.57	39.56	9.15E-04	43.65
±SD	6.73E-08	6.05	5.06	22.19	3.53E-04	3.70

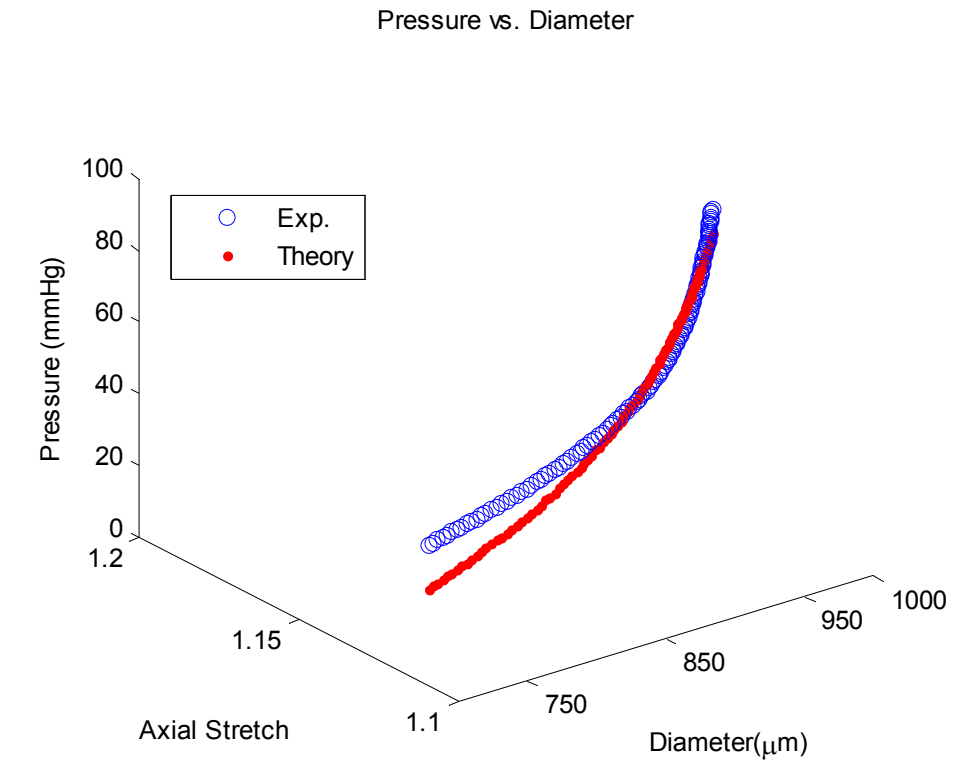

a

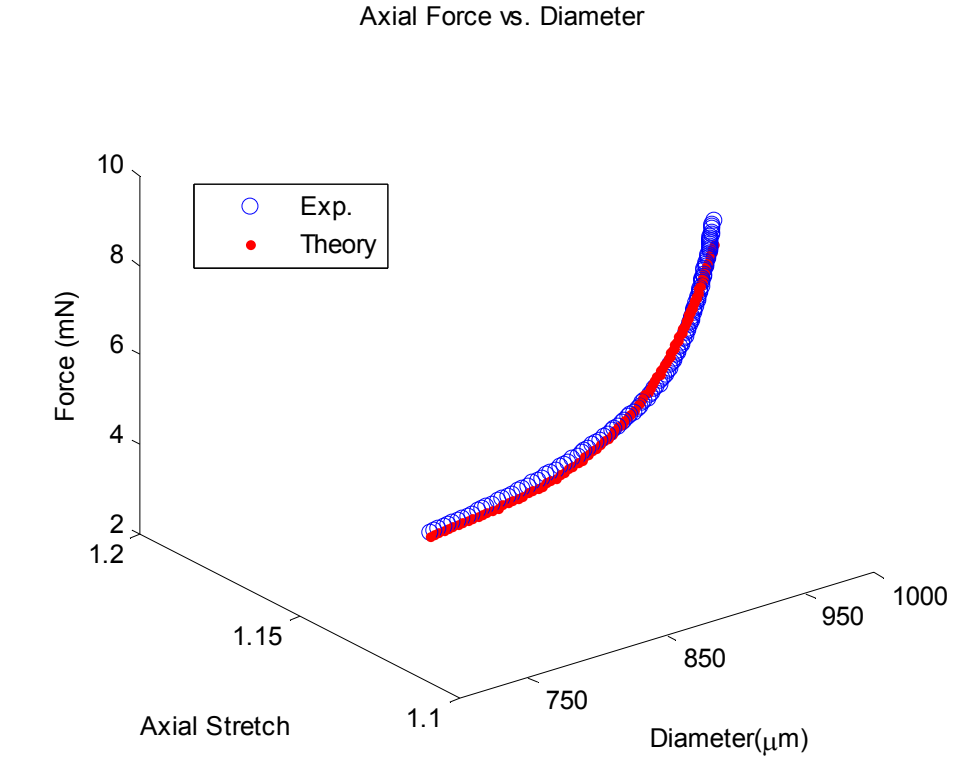

b

Fig. 21. Representative experimental data and model fits of the four fiber Holzapfel-type model at a stretch of 1.15. (a) Pressure-diameter plot. (b) Axial force-diameter plot.

DISCUSSION

Mechanical Testing

Hayashi et al.[19,20] and Monson et al.[25,26] reported important differences between intracranial and peripheral arteries: higher stiffness parameters, unique stiffness trends with aging, and less axial extensibility. However, to gain an accurate perspective on the mechanics of the cerebral vasculature from which to interpret normal function and pathogeneses, it is necessary to catalogue the biaxial response for vessels in physiologic conditions and orientations. The generated circumferential stress-stretch and force-pressure curves verify that pressure, diameter, and axial force measurements can be consistently recorded in our system for intact basilar arteries (Figures 10-13). Recorded circumferential stress values for vessels at 80 mmHg and 1.15 stretch were on the order of 120 kPa. Hayashi et al.[20] reported values for the human basilar artery at 100 mmHg to be around 196 kPa, though there was no mention of axial load.

One obstacle to maintaining control of the vessel's in vitro environment and accurate data measurement was the extensive branching of the basilar artery. The developed procedure for combining ligation with microsphere injection for occlusion of branches (cf. Figure 6) successfully stabilized the transmural pressure and isolated the intraluminal from the extraluminal environment. This method for pressure stabilization is faster and less detrimental to the live tissue when compared to cauterization or ligation alone. Less manipulation of the tissue and time under a microscope reduces the chances of tissue death or damage.

Extraluminal application of 60 mM KCl at 7 mmHg and no flow proved effective in producing maximum contraction of 30% and served as a quick and reversible way to

judge vessel viability. The 30% contraction in response to high KCl at low transmural pressure correlates well with contraction trends recorded by Vinall et al.[23] in bovine middle cerebral arteries. Mechanical testing under maximal contraction gives a framework for interpreting the contractile capacity of the wall. Quantification of contractile capacity and alterations therein will prove necessary for data interpretation in vasospastic vessel testing, but was beyond the current scope.

Axial force measurements verify in vivo stretch conditions and enhance our understanding of the vessel's axial mechanical properties. At in vivo stretches, axial force remains nearly constant despite increases in pressure[33,34,35]. Careful assessment of unloaded lengths each day prior to testing is important for accurate stretch calculations. It is possible for vessels to remodel axially to a new unloaded length during culture[40]. Testing at an increased or decreased stretch from the designated 'in vivo' stretch can shift the pressure-diameter curve (Figure 12) and result in inaccurate interpretation of data.

Mechanical data of acute and cultured vessels (Figure 13) validate the ability of our system to maintain physiologic conditions during the culture period. The data on Day 2 of culture closely resembled the acute data (Day 0), suggesting no alterations in mechanical properties of the vessel due to culture conditions. Any alterations recorded in cultured vasospastic vessels can therefore be attributed to the mechanisms of vasospasm and not as a result of stimulation from the culture system.

Imaging

As predictive models of arterial behavior continue to advance in complexity, there is an increasing need to include accurately the microstructural components of the artery wall. Not only can the microstructure of the artery provide important mechanical

information about the normal wall, it can also play an important role in disease conditions and pathological growth and remodeling. The distribution and orientation of collagen fibers throughout the artery wall, in particular, remains an important puzzle piece in the development of mathematical models. Collagen fibers are a key structural component of the arterial wall as they are the primary load-bearing constituent[3]. Hariton et al.[3] and Gasser et al.[4] note the importance of including collagen fiber orientation in the constitutive relations for remodeling analyses. The collagen fibers are thought to be primarily axially oriented in the adventitia, while in the medial layer a circumferential orientation dominates. A more precise descriptor of fiber distribution, however, is needed.

Nonlinear optical microscopy second harmonic generation provides unique microstructural information and allows imaging of live, intact arteries while maintaining in vivo geometries and conditions. The ability to image sequential layers throughout the thickness of the vessel wall at multiple pressures provides a way to quantify the collagen fiber orientation as a function of radius. The subsequent extraction of fiber angles from the images with Continuity is simple and elegant in comparison to polarized light microscopy (cf. Canham et al.[28], Finlay et al.[31], and Hu et al.[12]). Fiber orientation quantification depends strongly upon the pressure and stretch, variables that cannot be confirmed with high levels of accuracy in polarized light microscopy techniques such as pressure fixation, embedding, and sectioning. Validation of nonlinear optical microscopy for the imaging of collagen fibers motivates further exploitation of the technique to provide insight into structural adaptations both normal and pathogenic. Utilization of NLOM in culture is ideal as the vessel remains intact and requires no staining. Until now,

detailed information regarding the specific orientation of collagen fibers in the media and particularly in the adventitia has never been fully catalogued for the basilar artery.

A clear demarcation in fiber orientations between the media and the adventitia is clearly shown in the three dimensional histogram (Figure 15). The layers just past the 1/3 mark of the normalized position through the wall seem to suggest 'transition layers' between the adventitia and the media where there are both axial and circumferential fibers. We propose that this is an artifact of the curvature of the vessel. Visual inspection of the images shows a clear separation of the two layers with little, if any, transition zone. Also, the angle distributions of the adventitial layers did not get increasingly circumferential as the layers neared the media as certain mechanical models have suggested[3]. The dramatic difference in the mean angles further supports the structural distinction between the adventitia and media with no 'transition zone' (Figure 20). The mean fiber angle throughout the medial layer, near 90° at every slice, correlates well with the mean helical orientation (a value similar to α, Figure 8) of 88° reported in Finlay et al.[31] (angle value reference orientation altered for comparison). The authors, however, report a mean helical orientation for the adventitial layer of 37° at 120 mmHg, quite different from our mean helical calculation of 19.8°. This discrepancy could be an artifact of the previously discussed potential errors in pressure fixation and sectioning.

Modeling

The four fiber family model is preferred over purely phenomenological models[12] with its attention to microstructural components. Nevertheless, the fit to our data proved only fair (Figure 21). The parameters c, $c_1^{1,2}$, $c_2^{1,2}$, and $c_1^{3,4}$ compare well with those of Baek et al.[41] and Hu et al.[12], however, $c_2^{3,4}$ is significantly different. The low value of $c_2^{3,4}$

in comparison to $c_2^{1,2}$ reported here and to the similar parameter in Hu et al.[12] and $c_3^{2,3}$ in Baek et al.[41] may suggest that the collagen in the axial and circumferential directions could have a higher degree of undulation in comparison to the diagonal fibers in the pressure range of 7-80 mmHg. Visual inspection of the imaging data (Figure 14), however, contradicts this conclusion as the circumferential fibers at 40 mmHg and 80 mmHg (seen in images (d) at both pressures) has no detectable undulation. The discrepancies between reported parameters may also be a function of testing conditions, for example, higher pressure ranges during testing could result in altered model fitting. The parameter of particular interest for our experimental data comparison is α, the pitch of the diagonal fiber families. One assumption in the four fiber family model is that the same fiber orientations hold throughout the thickness of the vessel wall, an assumption that does not match the observations of the imaging data presented here. Thus, for comparison, we averaged all angles in all layers of the averaged imaging data, excluding all angles in a ±5° range from axial and circumferential. The resulting average of 43.6°, which compares favorably to the mean model-predicted value of α, 43.65°. Baek et al.[41] reported an α value of 50.92°, which is comparable to our model predicted α, however, the average α value in Hu et al.[12] was 21.42°. Until now it has not been possible to compare the fiber orientations and distributions predicted by mathematical models to quantified orientations throughout the vessel wall of live, intact arteries. Such a comparison here suggests that although the current structural models can closely fit the mechanical data, an improvement in the modeling of the structural components is necessary.

Although one-layer constitutive models have the potential to incorporate detailed structural information[3,4], we feel that the clear fiber distinctions between the adventitia and media support the development of a structurally-motivated two layer model of the vascular wall. Layer-specific modeling has been explored in the literature[36,37,38]. A two-layer cylindrical model describing the elastic properties of carotid arteries was developed by von Maltzahn et al.[37]. The inner layer (medial) was treated as isotropic, while the outer layer (adventitial) was treated as anisotropic. Demiray et al.[36] presented a layered cylindrical shell model of the aorta, with an isotropic elastic adventitial layer and an orthotropic elastic medial layer. Holzapfel et al.[38] formulated a structure-based model, characterizing the vascular tissue as a collagen fiber-reinforced composite with two distinct fiber orientations in the media and the adventitia. Medial fibers were oriented at ±10° and adventitial fibers at ±40° (0° = circumferential). We propose an extension of the layered modeling of a fiber-reinforced material to include a more accurate description of collagen fiber orientation and distribution. Gasser et al.[4] proposed a von Mises distribution (a circular version of a normal distribution) of collagen fibers in their recent structural model, but noted the necessity of more detailed information on the vessel microstructure to assess the accuracy of the model. The imaging data presented here supports the approximation of collagen in the adventitial layer as normally distributed (Figure 18), while the narrow distribution in the media (Figure 19) suggests the collagen in this layer can be modeled by one circumferential fiber family (Figure 22).

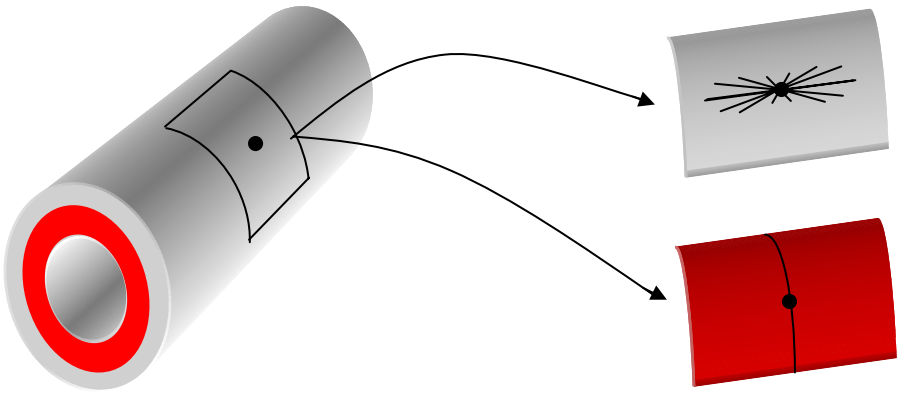

Fig. 22. Schema of proposed two layer model. The adventitial layer is in gray and has a normal fiber distribution. The media is in red and has one circumferential fiber family.

CONCLUSION

In addition to vasospasm, many pathogenic conditions involve structural and functional adaptation of the cerebral vasculature: cerebral aneurysm formation, arteriosclerosis, hypertension, and traumatic head injury. The work presented here will support a better understanding of the disease conditions through a more careful characterization of normal vascular mechanics and structural elements. The stress-stretch curves provide baseline characteristics for acute and short-term culture rabbit basilar arteries. The testing of maximally contracted arteries provides a framework for interpreting vessel basal tone in the culture system as well as a reference level of maximum activation to assess any alterations in contractile capability of vasospastic vessels (i.e. changes due to growth and remodeling). The quantified collagen fiber orientation has significantly contributed to the characterization of the normal vasculature microstructure and will support the development of accurate mathematical models connecting mechanical behavior and microstructural elements. Alterations in collagen fibers seen during growth and remodeling processes can also now be investigated.

REFERENCES

[1]Borel CO, McKee A, Parra A, Haglund MM, Solan A, Prabhakar V, Sheng H, Warner DS, Niklason L: Possible role for vascular cell proliferation in cerebral vasospasm after subarachnoid hemorrhage. Stroke 2003; 34:427-432

[2]Congenital and Traumatic Intracranial Aneurysms. Clinical Symposia 1977; 29(4): 1-40

[3] Hariton I, deBotton G, Gasser TC, Holzapfel GA: Stress-driven collagen fiber remodeling in arterial walls. Biomech Model Mechanobiol 2006; 6(3): 163-175

[4] Gasser TC, Ogden RW, Holzapfel GA: Hyperelastic modelling of arterial layers with distributed collagen fibre orientations. J R Soc Interface 2006; 3: 15-35

[5]Dumont AS, RJ Dumont, MM Chow, C-L Lin, T Calisaneller, KF Ley, NF Kassell, KS Lee: Cerebral vasospasm after subarachnoid hemorrhage: Putative role of inflammation. Neurosurg 2003; 53: 123-135

[6]Liu-DeRyke X, Rhoney DH: Cerebral vasospasm after aneurysmal subarachnoid hemorrhage: An overview of pharmacologic management. Pharmacotherapy 2006; 26(2):182-203

[7] Kuwayama A, Zervas NT, Belson R, Shintani A, Pickren K: A model for experimental cerebral arterial spasm. Stroke 1972; 3: 49-56

[8] Gleason RL, Gray SP, Wilson E, Humphrey JD: A multiaxial computer-controlled organ culture and biomechanical device for mouse carotid arteries. Biomech Eng 2004; 126: 787-795

[9] Tsurutani H, Ohkuma H, Suzuki S: Effects of thrombin inhibitor on thrombin-related signal transduction and cerebral vasospasm in the rabbit subarachnoid hemorrhage model. Stroke 2003; 34:1497-1500

[10] Salom JB, Torregrosa G, Alborch E: Endothelins and the cerebral circulation. Cerebrovasc Brain Metab Rev. 1995; 7(2):131-152

[11] Yamaguchi-Okada M, Nishizawa S, Koide M, Nonaka Y: Biomechanical and phenotypic changes in the vasospastic canine basilar artery after subarachnoid hemorrhage. J App Physiology 2005; 99:2045-2052

[12] Hu J-J, Baek S, Humphrey JD: Stress-strain behavior of the passive basilar artery in normotension and hypertension. J Biomech 2007; In Press

[13]Knoepp L, Bagwell CD, Garlich P, Brophy CM: Thrombin contraction of vascular smooth muscle: Implications for vasospasm. J Surg Inv 1999;1(4): 285-290.

[14]Yanamoto H, Sakai N, Sakai H, Xue J-H, Kikuchi H, Nagata I, Zhang Z: Broad-spectrum and selective serine protease inhibitors prevent expression of platelet-derived growth factor-BB and cerebral vasospasm after subarachnoid hemorrhage. Stroke 2001; 32:1665-1672.

[15]Nagasawa S, Handa H, Naruo Y, Watanabe H, Moritake K, Hayashi K: Experimental cerebral vasospasm. Part 2. Contractility of spastic arterial wall. Stroke 1983; 14(4):579-584

[16]Kim P, Sundt T, Vanhoutte P: Alterations in mechanical properties in canine basilar arteries after subarachnoid hemorrhage. J. Neurosurg 1989; 71: 430-436

[17]Nagasawa S, Handa H, Naruo Y, Moritake K, Hayashi K: Experimental cerebral vasospasm arterial wall mechanics and connective tissue composition. Stroke 1982; 13(5): 595-600

[18]Nagasawa S, Handa H, Okumura A, Naruo Y, Okamoto S, Moritake K, Hayashi K: Mechanical properties of human cerebral arteries: Part 2. Vasospasm. Surg. Neurol 1980; 14: 285-290

[19]Hayashi K, Handa H, Nagasawa S, Okumura A, Moritake K: Stiffness and elastic behavior of human intracranial and extracranial arteries. J Biomechanics 1980; 13:175-184

[20]Hayashi K, Nagasawa S, Naruo Y, Okumura A, Moritake K, Handa H: Mechanical properties of Human Cerebral Arteries. Biorheology 1980; 17(3): 211-218

[21]Moritake K, Handa H, Okumura A, Nagasawa S, Naruo Y: Quantitative analysis of microstructural components of human cerebral arteries. Neurological Res 1981; 3(1): 67-82

[22]Hogestatt ED, Andersson KE, Edvinsson L: Mechanical properties of rat cerebral arteries as studied by a sensitive device for recording of mechanical activity in isolated small blood vessels. Acta Physiol Scand 1983; 117:49-61

[23]Vinall PE, Simeone FA: Whole mounted pressurized in vitro model for the study of cerebral arterial mechanics. Blood Vessels 1987; 24:51-62

[24]Ohta T, Mori M, Ogawa R, Tsuji M: Development of a new perfusion system for pharmacological study on rabbit basilar arteries. Stroke 1991; 22(3): 384-389

[25]Monson KL, Goldsmith W, Barbaro NM, Manley GT: Axial mechanical properties of fresh human cerebral blood vessels. Journal of Biomechanical Engineering 2003; 125: 288-294

[26]Monson KL, Goldsmith W, Barbaro NM, Manley GT: Significance of source and size in the mechanical response of human cerebral blood vessels. Journal of Biomechanics 2005; 38:737-744

[27]Walmsley JG, Campling MR, Chertkow HM: Interrelationships among wall structure, smooth muscle orientation, and contraction in human major cerebral arteries. Stroke 1983; 14(5): 781-790

[28]Canham PB, Whittaker P, Barwick SE, Schwab ME: Effects of pressure on circumferential order of adventitial collagen in human brain arteries. Can J Physiol Pharmacol 1992; 70: 296-305

[29]Rowe AJ, Finlay HM, Canham PB: Collagen biomechanics in cerebral arteries and bifurcations assessed by polarizing microscopy. J Vasc Res 2003; 40:406-415

[30]Megens RTA, Reitsma S, Schiffers PHM, Hilgers RHP, De Mey JGR, Slaaf DW, oude Egbrink MGA, van Zandvoort MAMJ: Two-photon microscopy of vital murine elastic and muscular arteries: Combined structural and functional imaging with subcellular resolution. J Vasc Res 2007; 44:87-98

[31]Finlay HM, McCullough L, Canham PB: Three-dimensional collagen orientation of human brain arteries at different transmural pressures. J Vasc Res 1995; 32: 301-312

[32]Larson AM, Yeh AT: Ex vivo characterization of sub-10-fs pulses. Optics Letters 2006; 31(11): 1681-1683

[33]Dobrin PB: Biaxial anisotropy of dog carotid artery: estimation of circumferential elastic modulus. J Biomech 1986; 19: 351-358

[34]Takamizawa K, Hayashi K: Strain energy density function and uniform strain hypothesis for arterial mechanics. J Biomech 1987; 20:7-17

[35]Weizsacker HW, Kampp TD: Passive elastic properties of the rat aorta. Biomed Technik 1990; 35: 224-234

[36]Demiray H, Vito RP: A layered cylindrical shell model for an aorta. Int J Engng Sci 1991; 29(1): 47-54

[37]von Maltzahn WW, Besdo D, Wiemer W: Elastic properties of arteries: A nonlinear two-layer cylindrical model. J Biomechanics 1981; 14(6): 389-397

[38]Holzapfel GA, Gasser TC, Stadler M: A structural model for the viscoelastic behavior of arterial walls: Continuum formulation and finite element simulation. Eur J Mech A-Solids 2002; 21: 441-463

[39]van Loon P: Length-force and volume-pressure relationships of arteries. Biorheology 1977; 14(4): 181-201

[40]Gleason RL, Wilson E, Humphrey JD: Biaxial biomechanical adaptations of mouse carotid arteries cultured at altered axial extension. J Biomech 2007; 40(4): 766-776

[41]Baek S, Gleason RL, Rajagopal KR, Humphrey JD: Theory of small on large: Potential utility in computations of fluid-solid interactions in arteries. Comput Methods Appl Mech Eng 2007; In Press

VITA

Name:	Bethany Kay Wicker
Address:	337 Zachry Engineering Center MS 3120 College Station, TX 77843
Email Address:	wickerbk@hotmail.com
Education:	B.S., Biomedical Engineering, Texas A&M University, 2005 M.S., Biomedical Engineering, Texas A&M University, 2007